PFC/RR-83-15

DOE/ET-51013-85
UC20

ACTIVE STABILIZATION AND START-UP COIL CHARACTERISTICS

by

R.J. Thome, R.D. Pillsbury, Jr., and W.R. Mann

Massachusetts Institute of Technology
Plasma Fusion Center
Cambridge, Massachusetts 02139

FOREWORD

This work was supported by the U.S. Department of Energy, Office of Fusion Energy under Contract number DEA-CO278ET51013. It was originally prepared as "Active Stabilization and Start-up" and had limited distribution as Appendix C to FED-INTOR/MAG/82-2, which was submitted as part of the U.S. contribution to Session V of INTOR, Phase IIA, Vienna, July 1982.

CONTENTS

1.0 INTRODUCTION

Vertical plasma movement is inherently unstable in tokamaks using an elongated plasma because creation of this shape requires a negative field index. The radial field component associated with the latter is directed such that the force on the plasma following a vertical displacement tends to increase the displacement.

Recent operating scenarios for tokamaks have considered the use of separate control coils to provide active vertical stabilization of the plasma. An initial rapid vertical plasma displacement would be stabilized by eddy currents induced in passive elements, then, as the induced field decays, a set of active coils would be excited to provide the required field. This would limit the power required for the control coils since they would require excitation on the time scale of the induced field decay and not on the time scale of the displacement. Coils are also under consideration to provide additional plasma voltage for start-up (so called "blip" coils).

The placement of coils to serve these functions is dependent on spatial demands imposed by other subsystems. The power and energy required by the coils to perform these tasks is critically dependent on their location and eddy current effects induced by their rapidly changing fields. The purpose of this study was to provide the means to estimate the power and energy requirements and to present the results of a preliminary investigation of the eddy current effects. A simplified criterion was developed for relating the characteristic decay time of the passive system to the charge time for the active system.

2.0 CONTROL COIL POWER AND STORED ENERGY WITHOUT EDDY CURRENT EFFECTS

This section will develop the means for estimating the power required and energy stored for a pair of PF coils which are to provide either a specified radial field, vertical field or rate of change of flux at the location of the plasma.

Figure 2.1 illustrates two coaxial control coils of radius "a" and with planes located at $z = \pm d$. Each coil is excited with I ampere turns. The plasma is assumed to be located in the $z = o$ plane at a radius, r_o, and the sketch at the right shows the coils in a space with dimensions normalized to r_o. The case shown is of interest for evaluating the ability of the coils to produce a vertical field, B_z at (r_o,o) or a specified total flux, ϕ, through a loop of radius r_o in the $z = o$ plane. The case of radial field, B_r, production at r_o will require one of the loop currents to be reversed.

2.1 Vertical Stabilization

Vertical stabilization of the plasma requires production of a radial field at the plasma location to interact with the plasma current and produce a z-directed restoring force. The coils shown in Fig. 2.1 will, therefore, be assumed to be excited in series with axial fields opposed. The radial field produced at (r_o,o) by the two coils may be shown to be related to the energy stored in the coils, E_o, in the following manner.

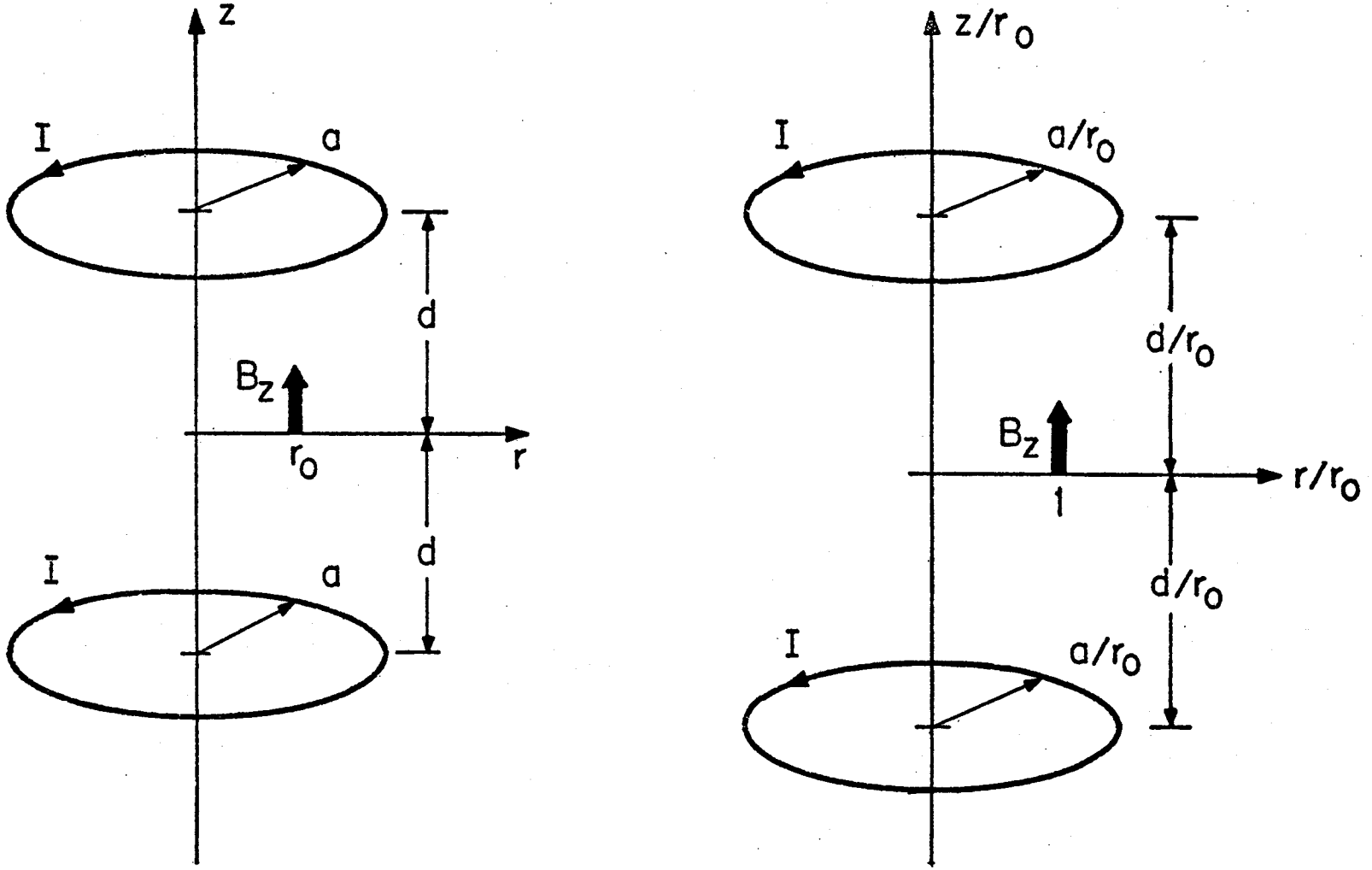

Figure 2.1 Illustration of a pair of control or start-up coils in real and in normalized space. The current directions shown correspond to the case where a vertical field is desired at r_o or a specified flux is desired through a loop of radius r_o in the z = o plane. For radial field production at r_o, the current direction in one loop should be reversed.

$$B_r = \sqrt{\frac{2\,\mu_o E_o}{r_o^3}}\; B_{re} \qquad (1)$$

where: $B_{re} = B_{re}\,(\rho, \eta, r_w/a)$

μ_o = permeability of free space = $4\pi \times 10^{-7}$ [H/m]

$\rho = a/r_o$

$\eta = d/r_o$

$\pi r_w^2 = A$

A = area of the envelope of the current carrying cross-section of one of the coils

The function B_{re} in Eq. (1) is dependent on the dimensionless location coordinates for the coils and a cross-sectional radius to coil radius parameter. B_{re} may be considered to be a normalized radial field and contours of constant B_{re} are shown in Fig. 2.2 for the case where $(r_w/a) = 0.05$. If a coil location is specified, then the contour value can be found from Fig. 2.2 and used in (1) together with the plasma radius, r_o, and required radial field, B_r to find the energy stored in the coils. Alternately, a region may be outlined on Fig. 2.2 showing the allowable areas for coil position based on other system interface constraints, then the coils can be located on the maximum contour. This location corresponds to the maximum radial field production capability for a given stored energy. Furthermore, the energy required for different locations may be compared by using ratios of the contour values for the locations. An example of this type will be presented in Section 4.0.

If the coil set has an initial current of zero, a characteristic time constant, τ_o, and is ramped at constant $\dot{I}$, then the power required at a time t_o after start is

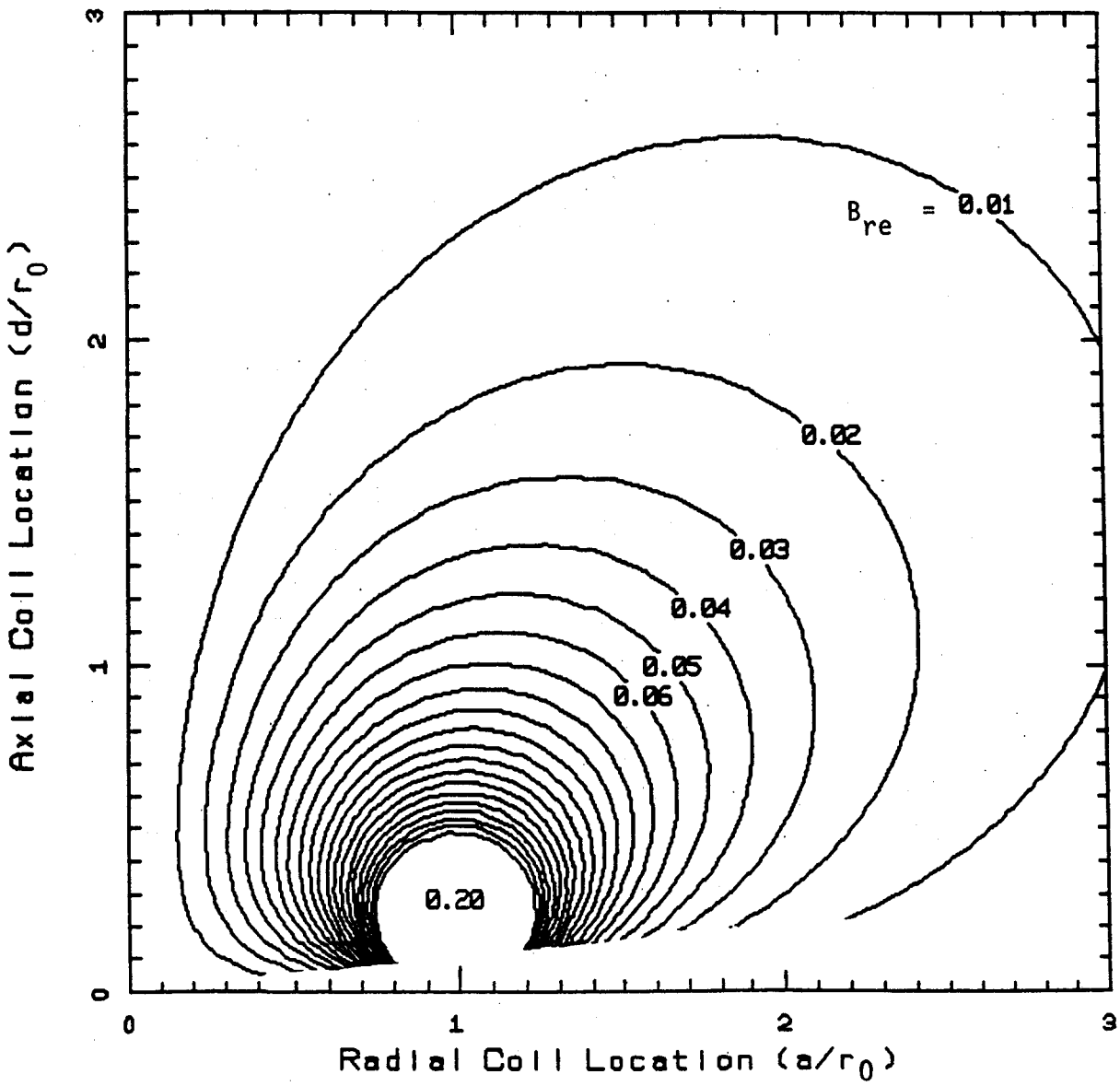

Figure 2.2 Contours of constant B_{re} for relating stored energy to radial field produced at $(r_o,0)$ which is at (1,0) in this diagram. (Note: contours are for $r_w/a = 0.05$)

$$P_p = \frac{2E_o}{t_o}\left[1 + \frac{t_o}{\tau_o}\right] \qquad (2)$$

where: P_p = power required at t_o while charging at a rate $\dot{I}$

E_o = stored energy

τ_o = (L-M)/R

L = self inductance of one coil

M = mutual inductance between coils

R = resistance of one coil

After E_o is determined by using (1) then the power required to achieve B_r in a time, t_o, may be found for a coil set of known τ_o by using (2). The time constant $\tau_o = \mu_o \sigma a^2 G_6$ where G_6 may be found from Fig. 2.3 when (r_w/a) is known.*

For cases where the coil set is cycled according to a specified current versus time scenario, the average power may be related to B_r as follows:

$$B_r = \mu_o \sqrt{\frac{P A_c}{r_o^3 \rho_{es}}}\, B_{rp} \qquad (3)$$

where: $B_{rp} = B_{rp}(\rho,\eta)$

P = average power

A_c = current carrying cross-sectional area of one coil

ρ_{es} = resistivity of coil material

---

* See R.J. Thome, R.D. Pillsbury, Jr., W.G. Langton, and W.R. Mann, "Coil and Shell Characteristics for Passive Stabilization," PFC/RR-83-14.

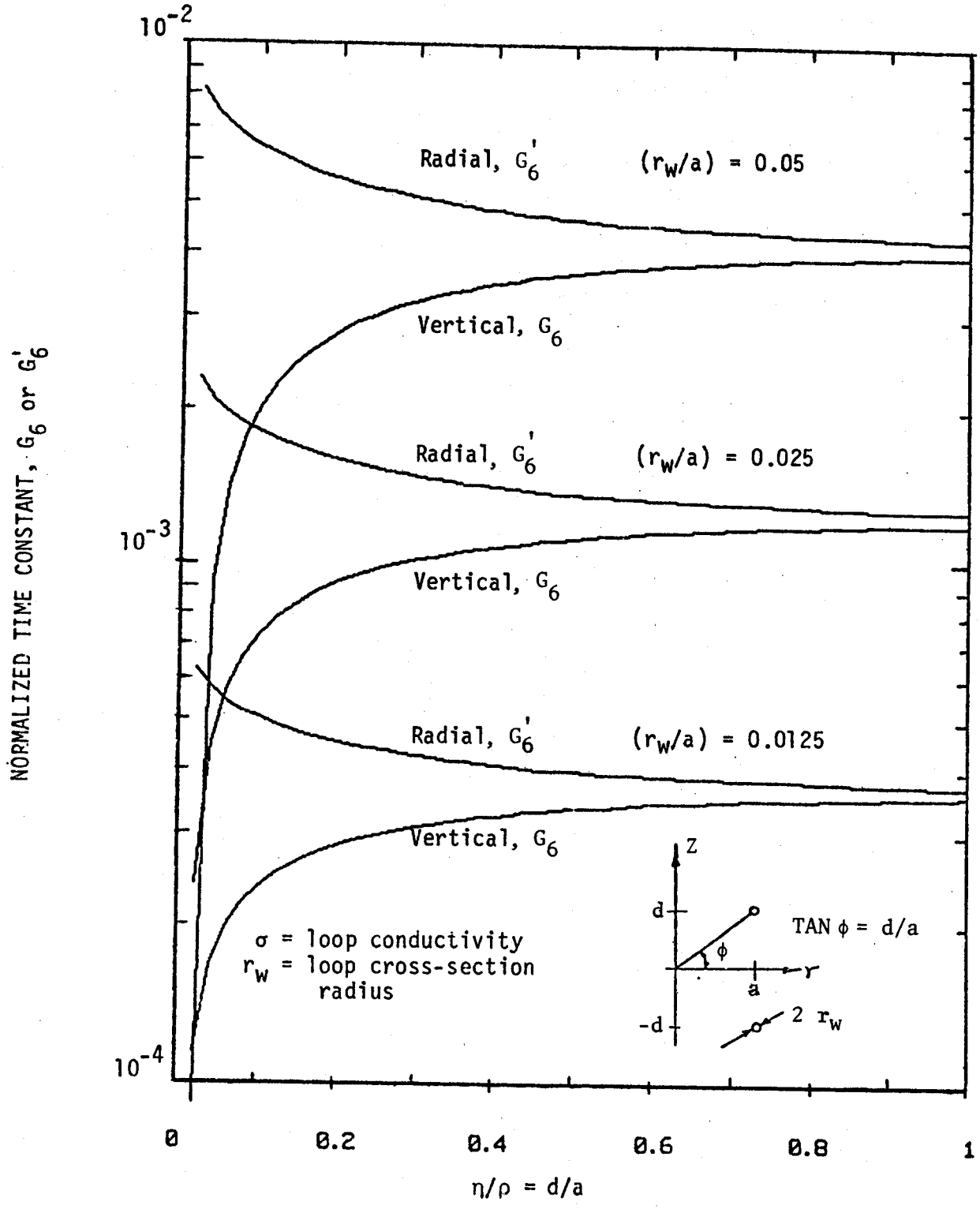

Figure 2.3 - Time constants for toroidally continuous loops.

The function B_{rp} may be considered to be a radial field normalized with respect to average power. Contours of constant B_{rp} are given in Fig. 2.4 and may be used to determine effective locations for vertical stabilization coils from the average power standpoint or comparing the average power requirements for alternate locations by using (3).

2.2 Radial Stabilization

Radial stabilization or control of the plasma requires production of a z-directed field at r_o, the plasma location, to interact with the plasma current and produce a radial restoring force. The coils shown in Fig. 2.1 will be assumed to be excited in series with axial fields aiding. The z-directed field produced at (r_o,o) by the two coils is given by:

$$B_z = \sqrt{\frac{2\ \mu_o E_o}{r_o^3}}\ B_e \qquad (4)$$

where: $B_e = B_e\ (\rho,\eta,r_w/a)$

Contours of constant B_e, the normalized z-field function, are plotted in Fig. 2.5. Coils on negative contours produce negative z-field at (r_o,o) when they are excited with positive current. Contours may be used in a manner similar to that described for (1) to determine energy requirements for coils at specified locations. The power required at t_o for a constant current ramp in this case may then still be found using (2), however, it is necessary to replace the time constant, τ_o, with

$$\tau_o \rightarrow \tau_o' = (L + M)/R \qquad (5)$$

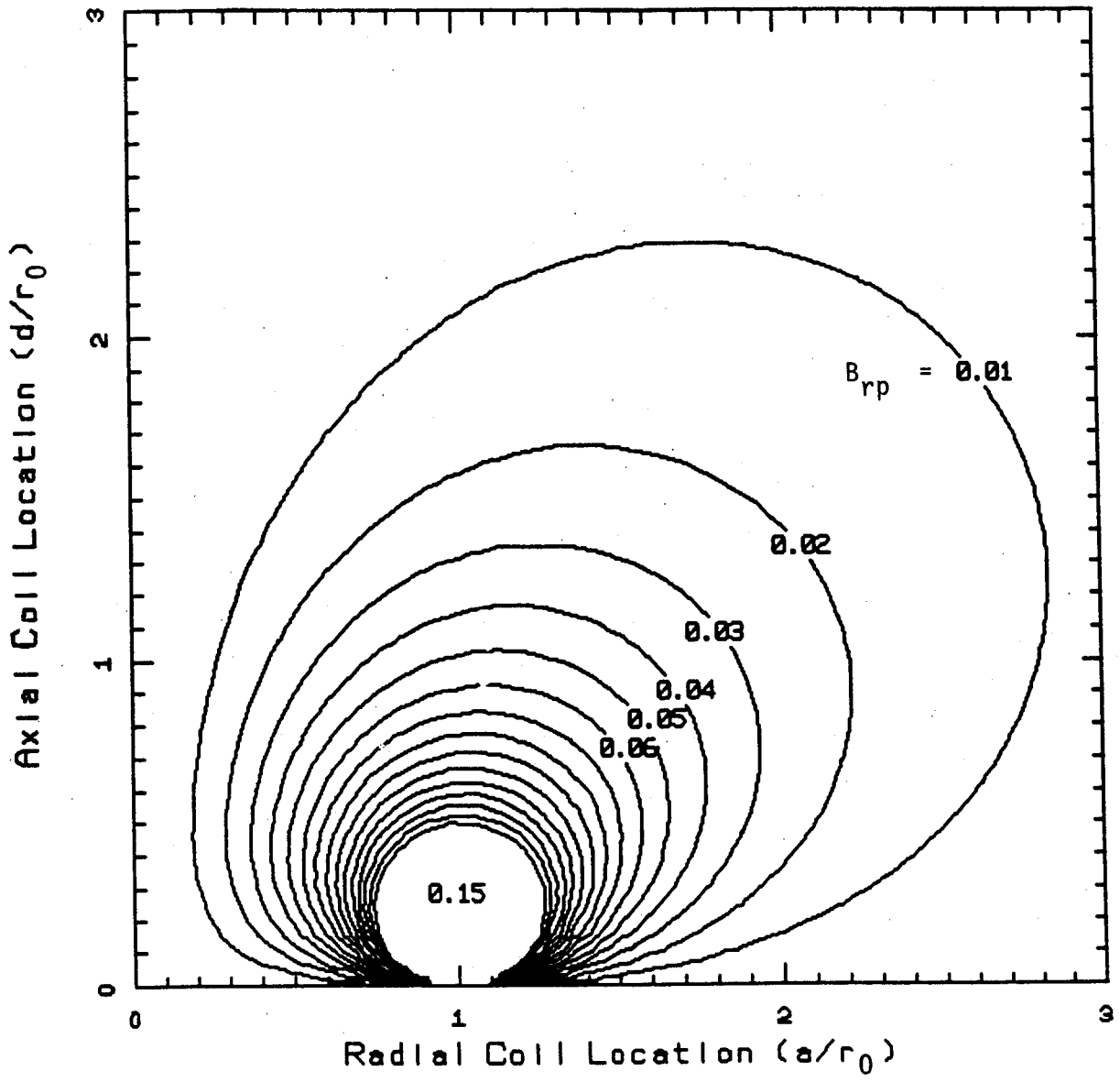

Figure 2.4 – Contours of constant B_{rp} for relating average power to radial field produced at $(r_0, 0)$ which is at (1,0) in this diagram.

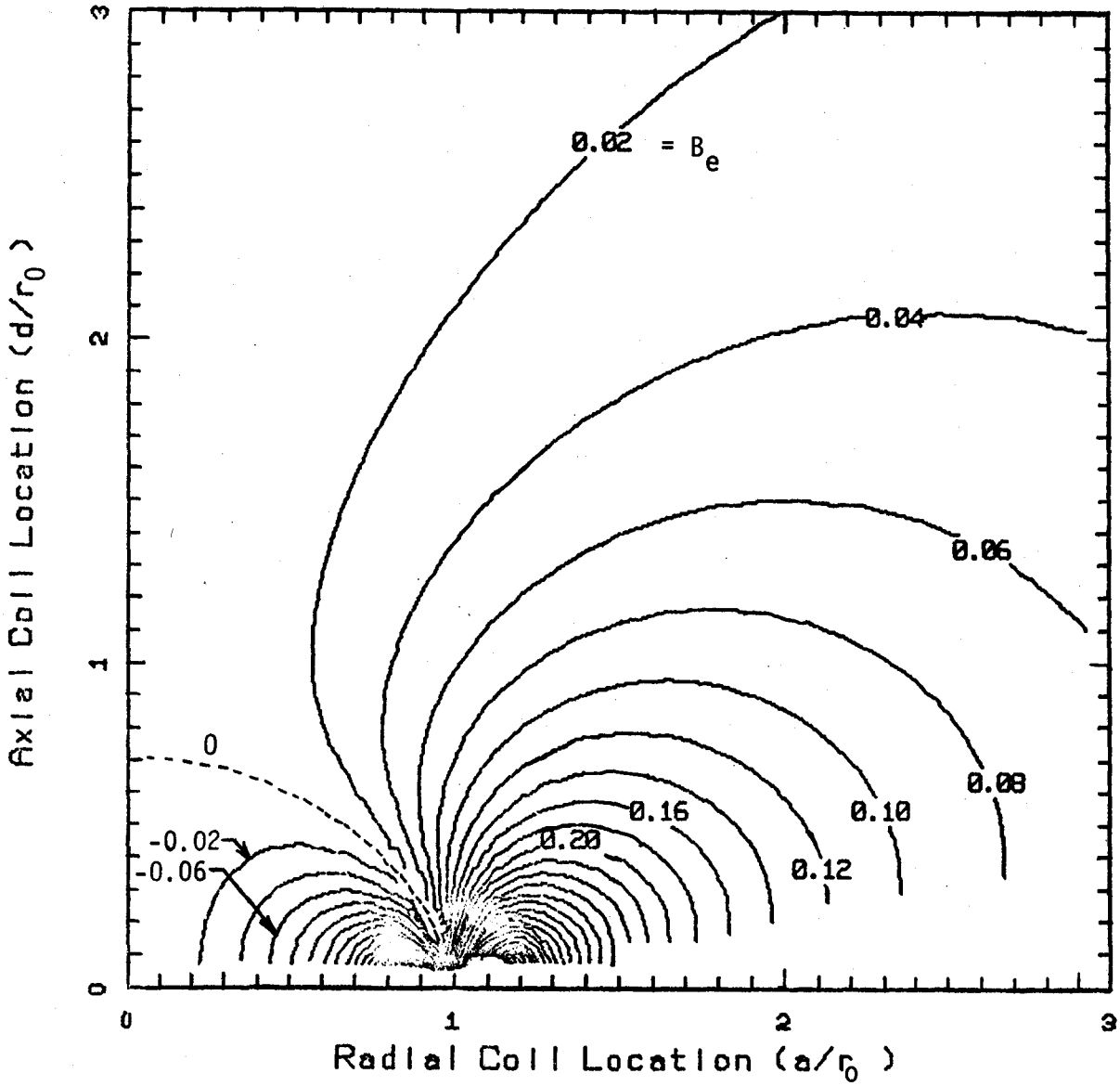

Figure 2.5 - Contours of constant B_e - see equation (4); A coil set on any given contour provides the same B_z for a given energy at a specified point $r = r_0$, $z = 0$ in real space or at $(d/r_0)=0$, $(a/r_0)=1$ in this figure ($r_w/a = 0.05$).

If the coil set is cycled according to a specified current vs time scenario, the average power, P, may be related to B_z as follows:

$$B_{\bar{z}} = \mu_o \sqrt{\frac{P\ A_c}{\rho_{es} r_o^3}}\ B_p \qquad (6)$$

where: $B_p = B_p(\rho,\eta)$

B_p is a normalized z-field function relative to average power. Contours of constant B_p are given in Fig. 2.6 and may be used in a manner similar to Fig. 2.4 to compare average power requirements for coils at different locations. Negative contours in Fig. 2.6 correspond to coil locations which generate negative z-field at (r_o,o) when they carry positive current.

2.3 Start-up

Coils used for start-up are required to produce a given rate of change of flux through the plasma loop in order to provide a driving voltage for a specified period of time. The required flux may be produced by two loops as shown in Fig. 2.1. They will be assumed to be connected in series, with z-field aiding.

The two loops produce an amount of flux ϕ which links the plasma contour of radius, r_o.

$$\phi = \sqrt{\mu_o r_o E_o}\ \ \Phi_e \qquad (7)$$

where: $\Phi_e = \Phi_e\ (\rho, \eta\ ,\ r_w/a)$

If the coil set is initially at current zero and is ramped at constant $\dot{I}$ to an energy E_o in a time t_o then the rate of change of flux, $\dot{\phi}$ is given by:

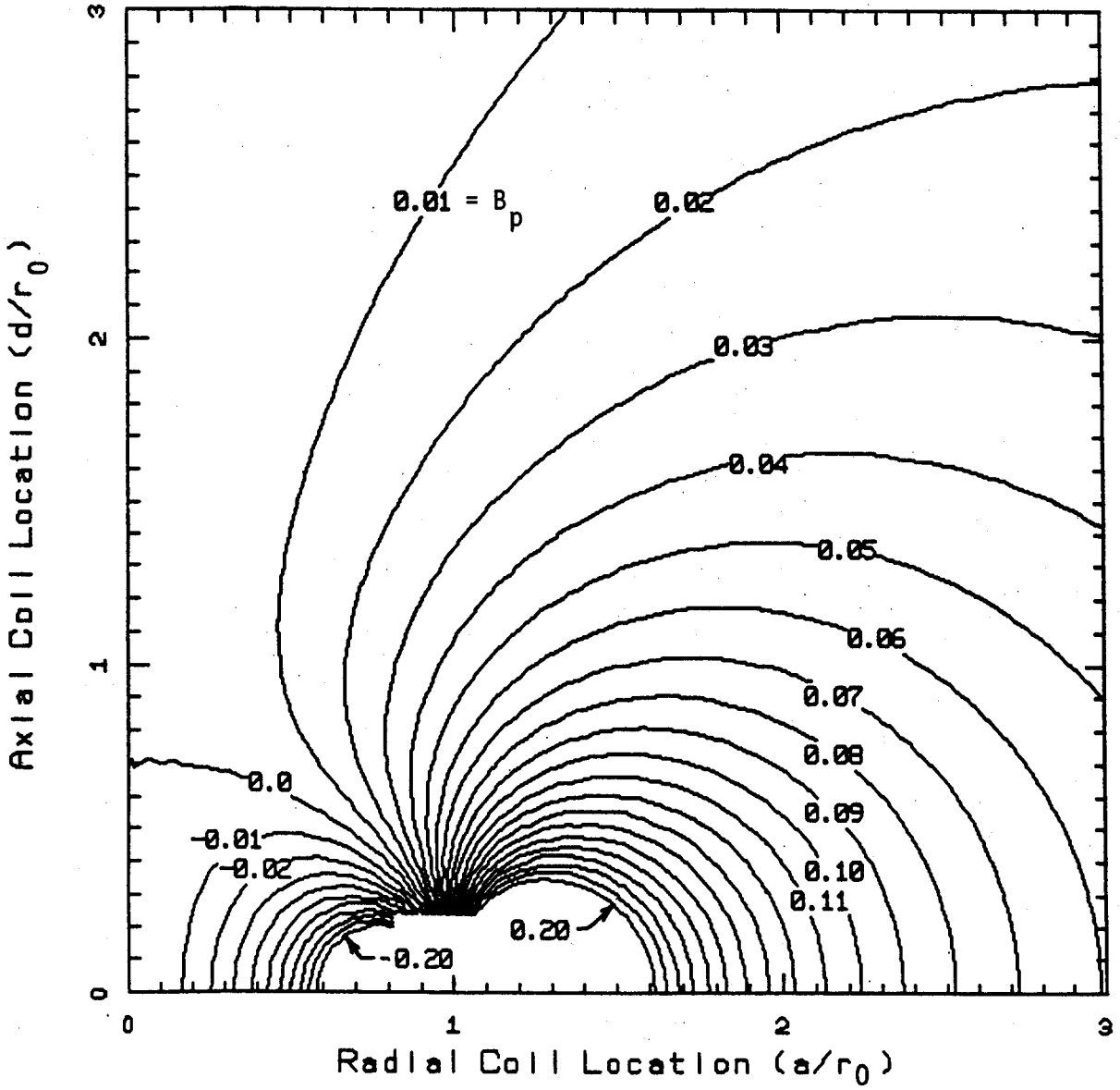

Figure 2.6 Contours of constant B_p for relating average power to Z-field produced at $(r_0,0)$ which is at (1,0) in this diagram.

$$\dot{\phi} = \sqrt{\frac{2\,\mu_o r_o E_o}{t_o^2}}\ \Phi_e \qquad (8)$$

Contours of constant Φ_e are shown in Fig. 2.7. A coil set of specified coordinates may be located in the diagram to find Φ_e which is then used with (8) to find the stored energy if a rate of change of flux $\dot{\phi}$, is to be maintained for a time t_o. The corresponding power required for the coil set may then be found using (2) and (5). As in cases described earlier, relative energy requirements for coils at different locations may be determined using ratios of contour values. Examples using these curves will be presented in Section 5.0.

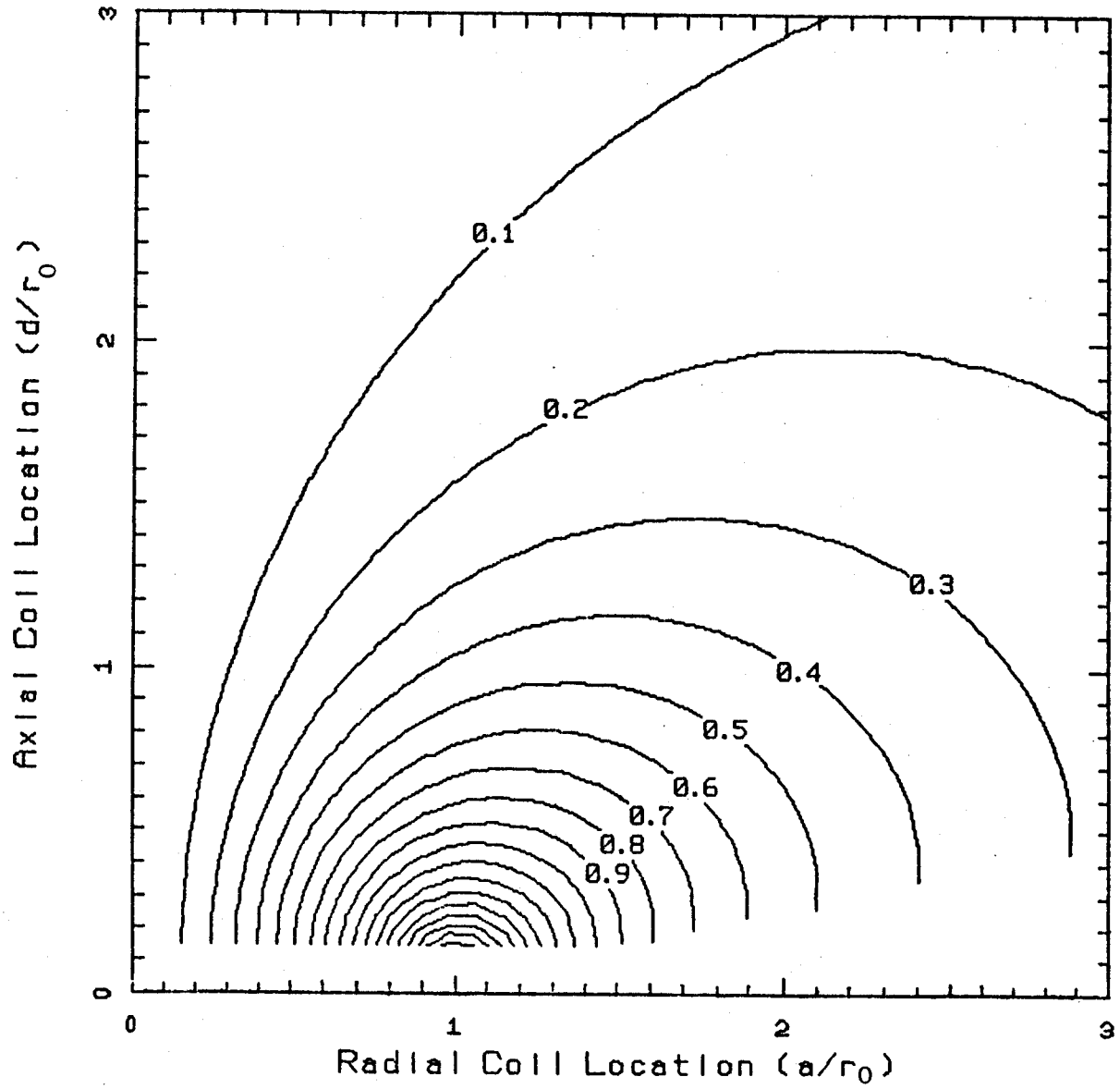

Figure 2.7 - Contours of constant Φ_e - see equation (8); coils located on a given contour produce the same normalized rate of change of flux through a contour of radius r_o in the z=0 plane ($r_w/a = 0.05$).

3.0 IMPACT OF INDUCED CURRENTS ON POWER AND ENERGY REQUIREMENTS

The previous section considered production of radial field and vertical field at the plasma and generation of a rate of change of flux through the plasma loop by a pair of discrete coils. Stored energy, average power and peak power were derived without consideration of induced currents in nearby conducting bodies. This section will present the results of a simple circuit model used to gain insight into the important parameters when eddy currents are induced in nearby conductors. Two time regimes are considered: 1) active coils charging with times short compared to passive time constants to respond to fast plasma displacements and 2) active coils charging with times long compared to passive element time constants as in start-up voltage assist. Consideration is given to criteria for relating the turn on time for active stabilization coils to the characteristic time constants for passive stabilizing materials and to the relationship of the simple parameters to quantities which can be computed using complex, finite element models. Results for the penetration time for field and flux through toroidal shells will then be presented as derived from computations using a finite element* model.

3.1 Two Coupled Circuits

3.1.1 Field and Flux Delay

Section 2.0 assumed that the magnetic field was being produced by a single circuit being driven by a power supply which could adjust its voltage as required to cause a current increase from zero at a constant rate of change. In this section, this primary circuit will still be assumed to be driven at constant $\dot{I}_1$. It will be assumed to have a self-inductance and resistance of

*R.D. Pillsbury, "A Two-Dimensional Planar or Axisymmetric Finite Element Program for the Solution of Transient or Steady, Linear or Non-Linear, Magnetic Field Problems", COMPUMAG, Chicago, Sept. 1981.

L_1 and R_1, respectively, and to be coupled through a mutual inductance, M, to a passive secondary circuit with self inductance and resistance of L_2 and R_2, respectively. The secondary circuit conceptually represents a conducting body in which eddy currents may be induced. If the initial current in both circuits is zero and if the primary is driven at constant $\dot{I}_1$ starting at t = o, then the current in the secondary will have the following form.

$$I_2 = - \left(\frac{M}{R_2}\right) \dot{I}_1 \left(1 - e^{-t/\tau_2}\right) \tag{9}$$

where:

$$\tau_2 = L_2/R_2$$

Equation (9) indicates that the secondary current rises from zero to a steady-state value with a time constant, τ_2. It should now be noted that if there were multiple secondaries, I_2 would have a sum of terms like the right side of (9) (ie - one for each secondary) as well as terms which arise due to inductive coupling between secondaries. The implication is that there is no single time constant for a complex system, however, if the primary is driven by constant $\dot{I}_1$ then the eddy currents will eventually reach a steady-state pattern.

The magnetic field at any point in space due to the two circuits may be expressed as

$$\overline{B} = \overline{\alpha}\, I_1 + \overline{\beta}\, I_2 \tag{10}$$

where $\overline{\alpha}$ and $\overline{\beta}$ are functions of the coordinates of the point where $\overline{B}$ is measured and of the spatial distribution of the wires in each circuit, but not of time. In most cases of interest to this effort $\overline{\alpha}$ and $\overline{\beta}$ will be positive. Equation (10), then, implies that the field at a point for a given time will always be less when the secondary is present since $I_2 < o$ as indicated by (9). If $\dot{I}_1$ is the same for two cases, one with and one without a secondary,

then the time lag to reach the same value of B_i at the point is

$$\Delta t_B = \left(\frac{\beta_i}{\alpha_i}\right) \frac{M}{R_2} \left\{ 1 - \exp\left[-(t + \Delta t_B)/\tau_2\right] \right\} \tag{11}$$

where α_i and β_i are the functions associated with the B_i component of $\overline{B}$. when $t >> \tau_2$, the time lag, Δt_B, reaches a constant value given by

$$\Delta t_{BS} = \left(\frac{\beta_i}{\alpha_i}\right) \frac{M}{R_2} \tag{12}$$

Equation (12) indicates that the time lag is not a function of $\dot{I}$ for $t >> \tau_2$, but is dependent on the location of the point relative to the two circuits through (β_i/α_i), on the location of the two circuits relative to one another through M and on the resistance of the secondary. Even though there is only one secondary, the time lag will not be the same for all points in space since (β_i/α_i) will, in general, not be a constant. Therefore, analysis of complex situations involving many shells (or secondaries) will eventually require that the time lag be evaluated for several points over an entire region of interest. Scaling of results must be limited to equivalent geometries with equivalent points, with Δt_{BS} inversely proportional to the resistance of the secondary circuits. In situations involving shells as secondary circuits, Δt_{BS} may be scaled proportional to the ratio of thickness to resistivity for the shells. The scaling must involve multiplying the thickness to resistivity ratio of all shells by the same constant in order to be valid, however.

If we consider the z-component of $\overline{B}$ in (10) then the flux linked by a contour coincident with the plasma loop of radius r_o in the z = o plane is given by the following when the primary is charged at constant $\dot{I}_1 = (I_o/t_o)t$:

$$\phi = 2\pi \, (I_o/t_o) \int_o^{r_o} \left[\alpha_z \, t - \beta_z \, (M/R_2) \, (1 - e^{-t/\tau_2})\right] r \, dr \tag{13}$$

The first term in the integrand in (13) arises from the primary alone. If the derivative of (13) is taken with respect to time it can be shown that $\dot{\phi}$ for the contour is the same with or without the secondary provided $t >> \tau_2$. Thus, the induced voltage in the plasma loop will eventually be the same with or without the secondary, however, there will be a time lag associated with the flux linked by the loop which, for $t >> \tau_2$, can be shown to be:

$$\Delta t_{\phi_s} = \frac{M}{R_2} \frac{\int_0^{r_o} \beta_z \, r \, dr}{\int_0^{r_o} \alpha_z \, r \, dr} \tag{14}$$

In general, the ratio of integrals in (14) will not be equal to (β_z/α_z) in (12), hence, the time lag for flux will not be the same as the time lag for field. All other comments on scaling made relative to (12) also apply to (14).

3.1.2 Active Stabilization

This section will consider the case of control coils which would respond faster than the PF system to stabilize the plasma. If the plasma moves suddenly, it will be initially stabilized by restoring forces generated by induced currents in the passive stabilization coils (or shells). As the current in the passive system decays, the stabilizing function will be assumed by the active control coil system.

In order to visualize the sequence of events, assume the passive stabilization system to be a single loop circuit consisting of an inductance, L_2 and resistance, R_2. The loop is inductively coupled to the plasma which undergoes an instantaneous displacement and induces a current I_{20} in the passive loop. The current then decays with a time constant, $\tau_2 = L_2/R_2$ as illustrated in Fig. 3.1 as the top curve. If, on the other hand, the same passive circuit has zero current initially and is inductively coupled to the control coils

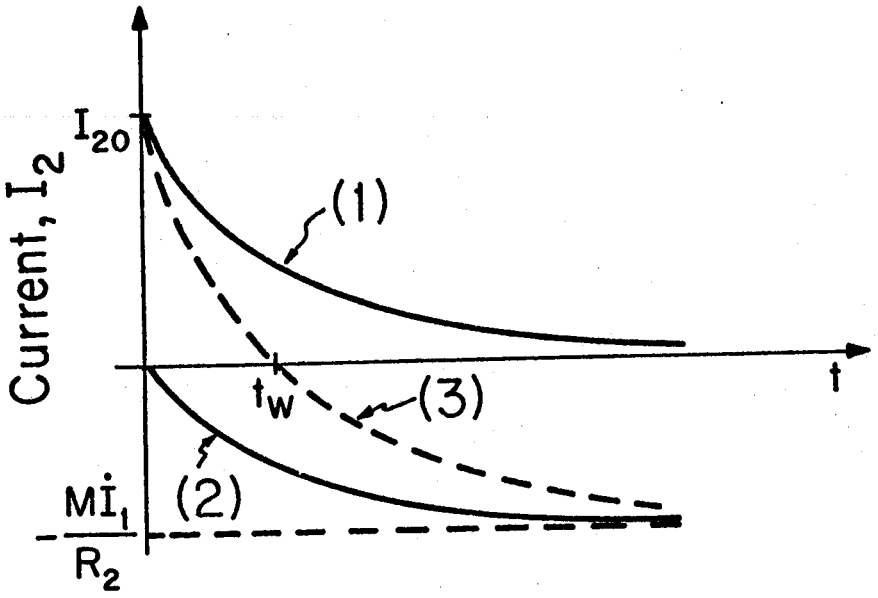

Figure 3.1 Current vs time in the passive stabilization system when driven by (1) a sudden plasma displacement only; (2) the control coils driven at constant $\dot{I}_1$ only or (3) a sudden plasma displacement and control coil activation at constant $\dot{I}_1$ simultaneously.

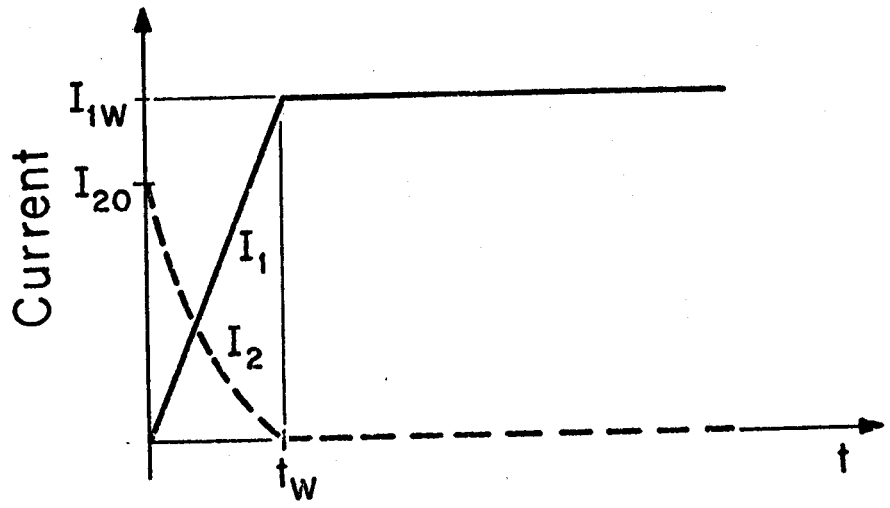

Figure 3.2 Postulated operating sequence where the active coil is ramped at constant $\dot{I}_1$ to $\dot{I}_{1W}$ in a time t_w when the passive circuit current is zero then $\dot{I}_1 = 0$ for $t > t_w$.

which are activated at t = 0 with a constant current ramp $\dot{I}$, then it will respond as indicated by (9) and as illustrated by curve (2) in Fig. 3.1. If both events occur then the current in the passive system will respond as shown by curve (3). The latter indicates that the increasing current in the control coil forces the current to decrease faster in the passive system and, ultimately, to become negative and approach the steady state value which can be found from (9).

Equation (10) describes the field at any point in space (e.g. - at the plasma) due to the two circuits. If both currents are positive, they add to the desired field. Curve (3) in Fig. 3.1 indicates that I_2 eventually becomes negative if $\dot{I}_1$ is ramped continuously. Therefore, we shall postulate that the desirable sequence of operations is as shown in Fig. 3.2, that is, to ramp I_1 until the time t_w when I_2 is zero, then hold I_1 constant at the value I_{1w}. In this way, both the passive and active coils contribute to the desired field at all times. Note that a more complex plasma model which includes some form of dynamic response may alter the criterion for specifying the time at which the active coil must be "on".

The ratio of the time, t_w, in Figures 3.1 and 3.2 to the time constant τ_2 may be shown to be determined by the following transcendental function.

$$\frac{t_w}{\tau_2} = \ln\left[1 + \frac{A}{(t_w/\tau_2)}\right] \tag{15}$$

where:

$$A = \left(\frac{B_o}{B_d}\ \frac{\Delta t_{BS}}{\tau_2}\right)$$

$$B_o = \beta I_{20}$$

$$B_d = \alpha I_{1w}$$

Δt_{BS} = time lag constant from (12)

In (15), B_o is the field initially induced by the plasma displacement and produced by the passive coil system and B_d is the field produced by the control coil after it is fully turned on. The ratio $B_o/B_d > 1$, but may be expected to be of order unity. The characteristic time lag Δt_{BS} may be expected to be several times τ_2, hence, A is also of order unity and is probably ≈ 3. Equation (15) is plotted as a function of A in Fig. 3.3 which indicates that it varies slowly in the range $1 < A < 5$ and that a value of ≈ 1 for estimating purposes is appropriate. This implies that the ramp time t_w, for the active coil should be approximately equal to the time constant of the passive system, τ_2. Now, the energy and peak power for the control system may be estimated.

First, specify a plasma radius, r_o and control coil location in Figure 2.2, then determine B_{re}, the radial field normalized to stored energy, from the contour value through the coil coordinate in normalized space. Let $B_r = B_d$, the desired field at the plasma from the control coil, and find E_o, the stored energy in the control coil pair from (1). The energy input to the control coils and peak power may then be estimated using the following:

$$E_{in} \lesssim E_o \left[1 + \frac{2}{3} \frac{t_w}{\tau_1}\right] \tag{16}$$

where: $\tau_1 = L_1/R_1$ = time constant for control coil circuit

$$P_p \lesssim \frac{2E_o}{t_w} \left(1 + \frac{t_w}{\tau_1}\right) \tag{17}$$

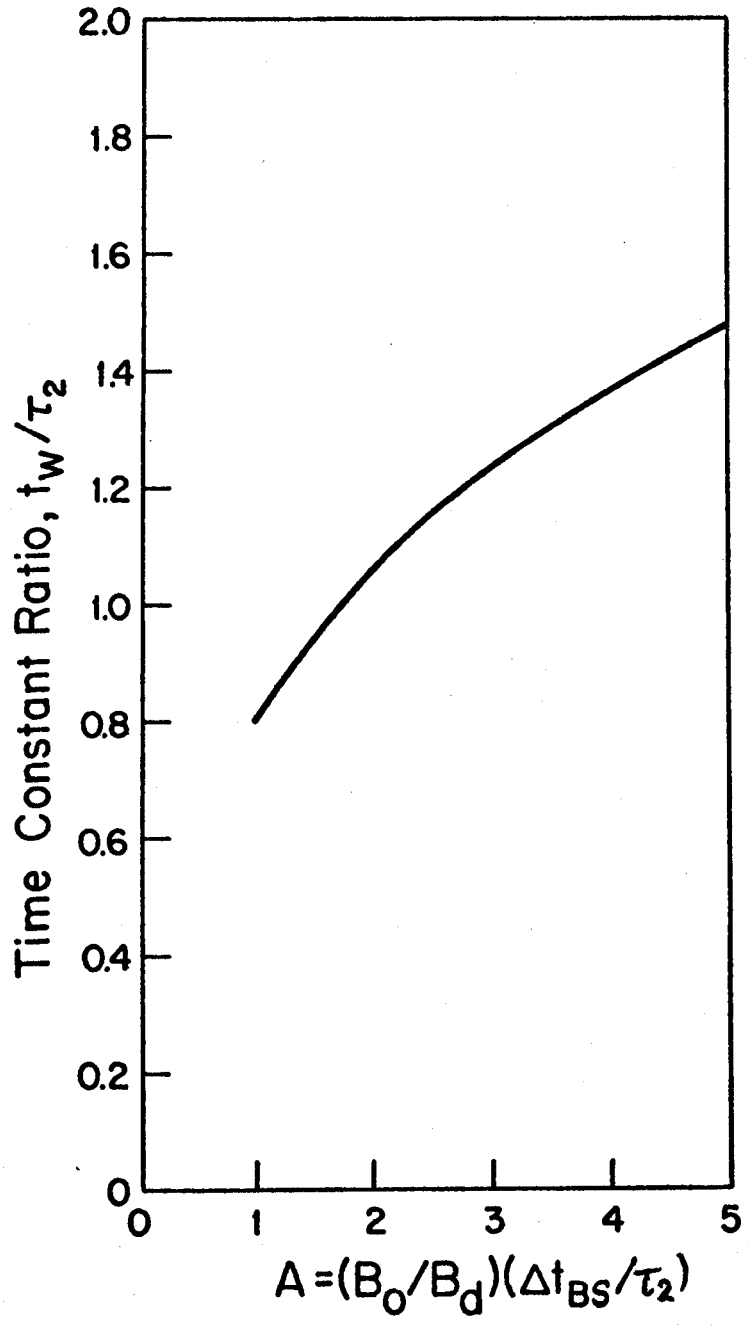

Figure 3.3 Charge time for active coil set as a function of system characteristics (see (17) and Figure 3.2).

This section has described the interaction between the active coil and passive stabilization elements in terms of a simple two circuit model in which the active coil is charged at constant $\dot{I}_1$ for $0 < t < t_w$. The passive system has simplified time characteristics described by τ_2 and Δt_{BS}, where, for estimation purposes, $t_w \approx \tau_2$. Continuous systems involving shells and other distributed conducting materials, however, do not have a single time constant. Section 3.2, therefore, will illustrate the means for relating the simple concepts to the output from a continuum model.

3.1.3 Start-up Voltage Assist

The start-up voltage problem may also be envisioned with the two loop circuit of Section 3.1.1. In this case the start-up coils are assumed to ramp at constant $\dot{I}_1$. Eddy currents induced in conducting materials may be modeled as a single passive circuit which then responds with the current I_2 given by (9). The flux penetration into the plasma circuit will be delayed by the eddy currents, hence, the start-up coils must ramp for a time $\Delta t_{\phi s}$ (see (14)) plus the necessary time interval for voltage application, t_v.

If the coil locations are known then the normalized flux function, Φ_e can be found from Fig. 2.7 by finding the value of the contour through the coil coordinates. This value may then be used with the plasma radius (r_o), voltage ($\dot{\phi}$), and time t_v in (8) to find E_o, the stored energy in the start-up coils when charged for a time $t_v = t_o$. The energy input to the start-up coils after charging for the required time of $(t_v + \Delta t_{\phi s})$ may then be estimated from

$$E_{in} \lesssim E_o \left(1 + \frac{\Delta t_{\phi s}}{t_v} \right)^2 \left[1 + \frac{2}{3} \frac{t_v}{\tau_1} \left(1 + \frac{\Delta t_{\phi s}}{t_v} \right) \right] \qquad (18)$$

Sample results based on (18) and coils located using Fig. 2.7 will be given in Section 4.0.

3.2 Penetration of Field and Flux Through Shells

Section 3.1.1 showed that the time lag for field generation at a point and the time lag for flux generation through a contour, due to a coil set driven at constant $\dot{I}$, are not equal and are dependent on the geometry and location of the active coils as well as the passive conductors. This section will summarize the results from a finite element model used to estimate typical time lags for field and flux, which will then be used in Section 4.0 to arrive at peak power and energy estimations for the control and start-up coils considered in Section 2.0 with corrections for eddy current effects.

The conductors in the axisymmetric finite element model are shown in Fig. 3.4. The model utilized three toroidal shells which are shown as solid lines and three coils designated as inside-inboard (II), inside-outboard (IO) and outside-outboard (OO). Three of the boundaries for INTOR are shown using dashed lines. Figure 3.5 is similar, but shows two of the boundaries for the FED baseline.

Cases were run in which one of the coils was excited at constant $\dot{I}$ and the z-directed field at the plasma center as well as flux through the plasma loop were computed as a function of time. Typical results are shown in Fig. 3.6 which shows four curves. The curve labeled "no shells" is the solution for coil excitation alone without eddy currents in the shells. The curve labeled "cryostat only" assumes that the inner two shells have infinite resistivity and, therefore, no eddy currents. The other two curves assume that all three shells are present, but shows the effect of a resistivity change for the two inside shells. In all cases, the effect of the eddy currents is to

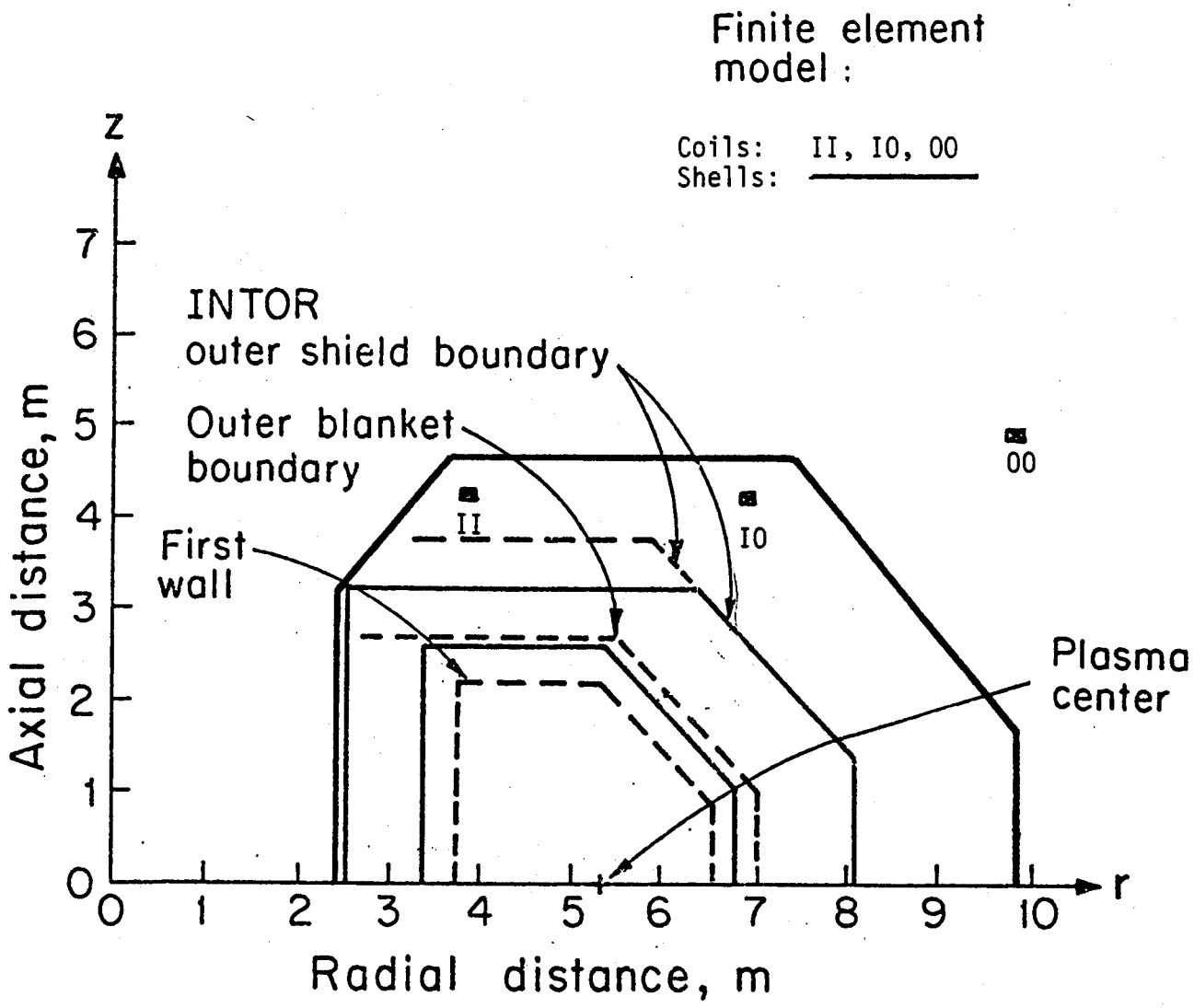

Figure 3.4 - Sketch of Three INTOR boundaries superimposed on a Finite Element Model Composed of Three Conducting Shells and Three Coils.

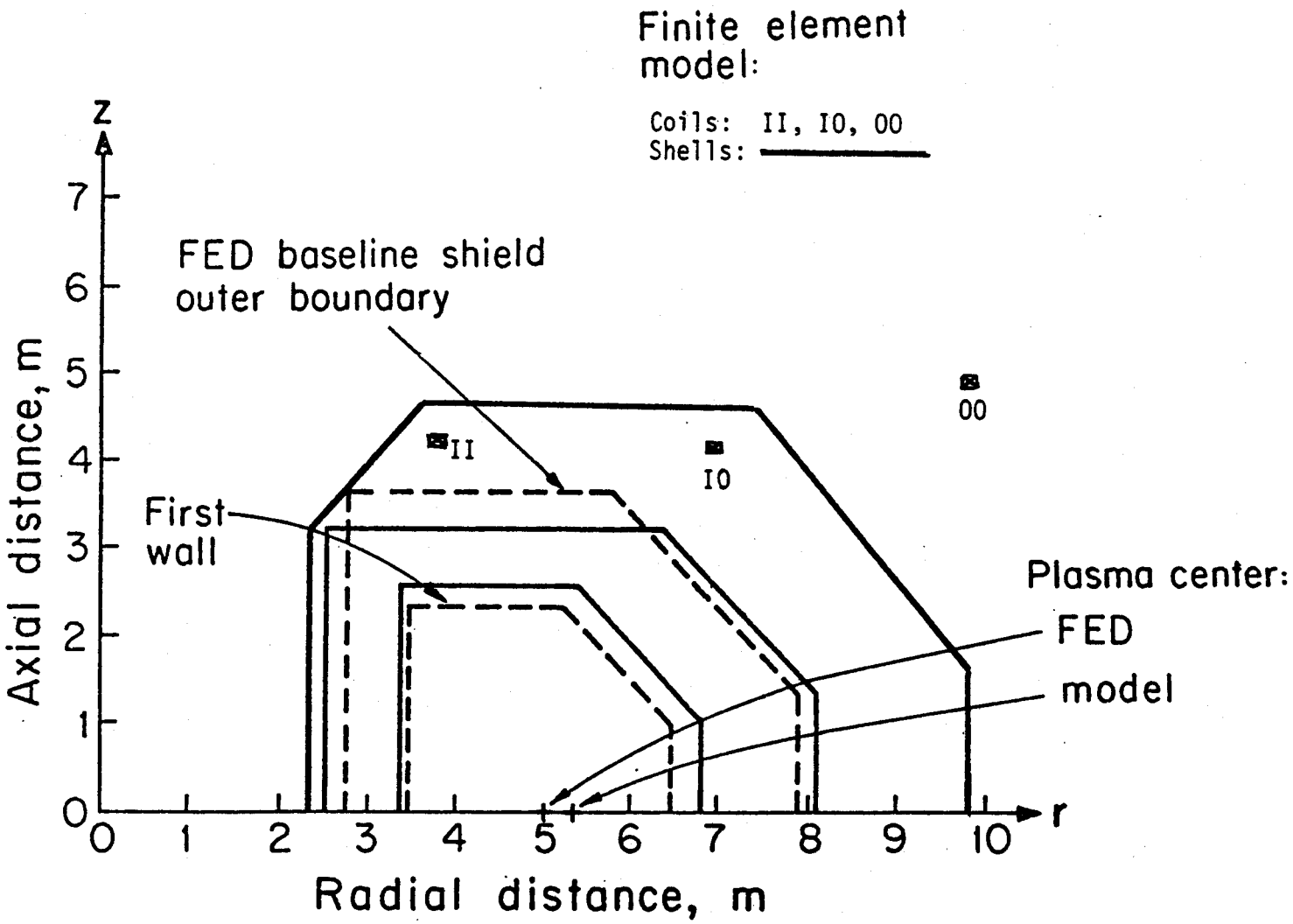

Figure 3.5 - Sketch of 3 FED boundaries superimposed on a finite element model composed of three conducting shells and three coils.

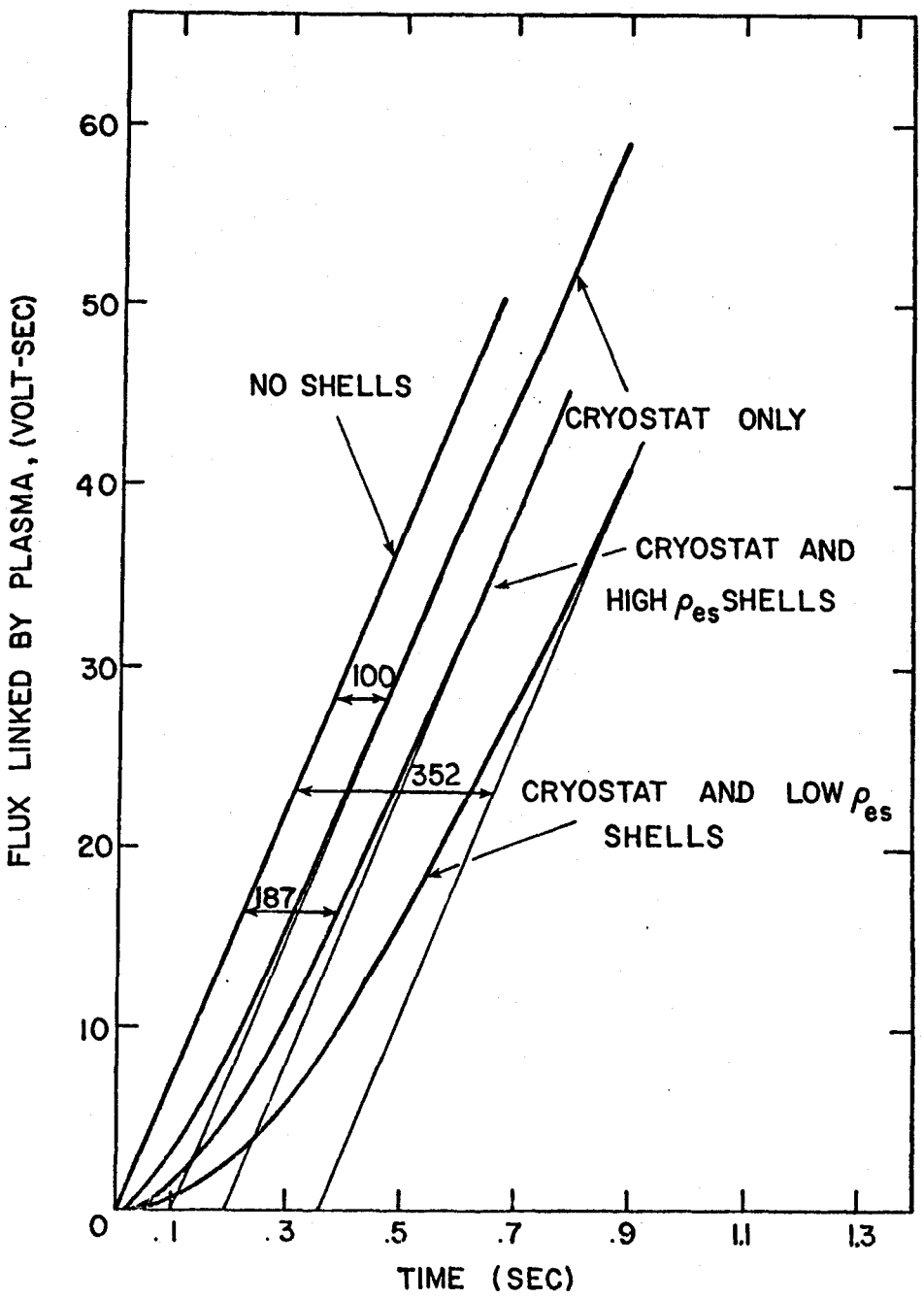

Figure 3.6 Typical results for flux vs time due to constant $\dot{I}$ excitation of coil 00 for three cases of shell resistance.

lead to a time lag which eventually becomes constant and corresponds to Δt_{ϕ_s} in (14).

The time lag for the "cryostat only" or outside shell was 100 msec when driven by coil 00 alone and 62 msec when driven by coil 10 alone. This shell included a shell thickness to resistivity ratio, (t_s/ρ), which varied poloidally to account for differences in actual wall thicknesses and to make a first order correction for openings in the shell on the outboard side. Table 3.1 summarizes the characteristics of this shell which was unchanged between cases. The last column gives the equivalent thickness for a toroidally continuous stainless steel shell.

The time lag for field and for flux for the cases which were run are summarized in Table 3.2. In all cases the outer shell values were held constant as in Table 3.1 and only one coil was excited. In all cases considered, $\Delta t_{B_s} < \Delta t_{\phi_s}$, however, they are comparable in size. The time lag for the 10 coil is less than that for the 00 coil in all cases and the difference is more pronounced for thinner shells. The model assumes toroidal continuity of all shells. If the two inner shells are sectored to prevent net current flow through the rz-plane then the time lags are estimated to decrease by ≈ 2 for cases where $t_s > 0$, but with the time lag for $t_s = 0$ as a lower limit.

Table 3.1 - Characteristics of Outside Shell in Finite Element Model

Shell Segment	from coord (r, z)	to coord (r, z)	t_s/ρ $-\Omega^{-1}$	$t_s\|_{ss}$ cm
inboard	2.5, 0	2.5, 3.23	2.82×10^4	2.73
top	2.5, 3.23	8.06, 4.03	7.1×10^3	0.7
outboard	8.06, 4.03	9.9, 0	3.88×10^4	3.77

Table 3.2 - Lag Time for Field and Flux at the Plasma Center[1]

Coil	inner shell[2]		mid-shell		Δt_{ϕ_s}[3]	Δt_{B_s}[3]
	t_s (cm)	ρ (10^{-6} Ω cm)	t_s (cm)	ρ (10^{-6} Ω cm)	(sec)	(sec)
00	3.2	122	3.2	72	352	315
	1.0	390	1.0	230	187	180
	0	∞	0	∞	100	—
I0	3.2	122	3.2	72	312	285
	1.0	390	1.0	230	138	131
	0	∞	0	∞	62	—
II	3.2	122	3.2	72	265	—
	1.0	390	1.0	230	142	—

(1) characteristics of outer shell are given in Table 3.1.

(2) inner shell resistivity increased by 1.7 to account for added peripheral length of convolutions.

(3) model assumes toroidal continuity of both shells; if both shells are sectored then time lags decrease by ≃2 for $t_s>0$ but with the $t_s = 0$ value as a lower limit.

4.0 EXAMPLES

This section will illustrate the use of the material developed in Sections 2 and 3 to estimate the characteristics of two active loops for plasma stabilization and for voltage start-up assist in INTOR. Four potential loop locations will be considered. These are located on the following boundaries: (1) the shield outer boundary; (2) the plasma side of the TF coil; (3) the TF coil outer boundary; and (4) a curve which passes through the approximate centers of the PF coils in an rz-plane.

The four boundaries are shown in Fig. 4.1. It is assumed that the blanket is 0.5 m thick, the shield is 1.0 m thick and that there is a 0.1 m gap between blanket and shield. The TF and PF coil boundaries are based on the INTOR Phase I design.*

4.1 Vertical Stabilization

Figure 4.1 shows contours of constant dimensionless radial field produced by a pair of coils as well as the four boundaries of interest. The points labelled A, B, C and D correspond to the location on the four boundaries where a coil should be placed to produce the maximum radial field at the plasma for a given stored energy in the coil pair. Possible locations at radii less than the inboard first wall are ignored for this exercise, due to the limited space available.

Table 4.1 gives the four points, their locations, and their radial and axial coordinates for an assumed plasma major radius of 5.3 m. The fifth entry in the table gives the dimensionless radial field value. If the desired field at the plasma is specified then the energy stored by the coils can be

---

* International Tokamak Reactor: Phase One, Report of the International Tokamak Reactor Workshop, IAEA, Vienna, 1982.

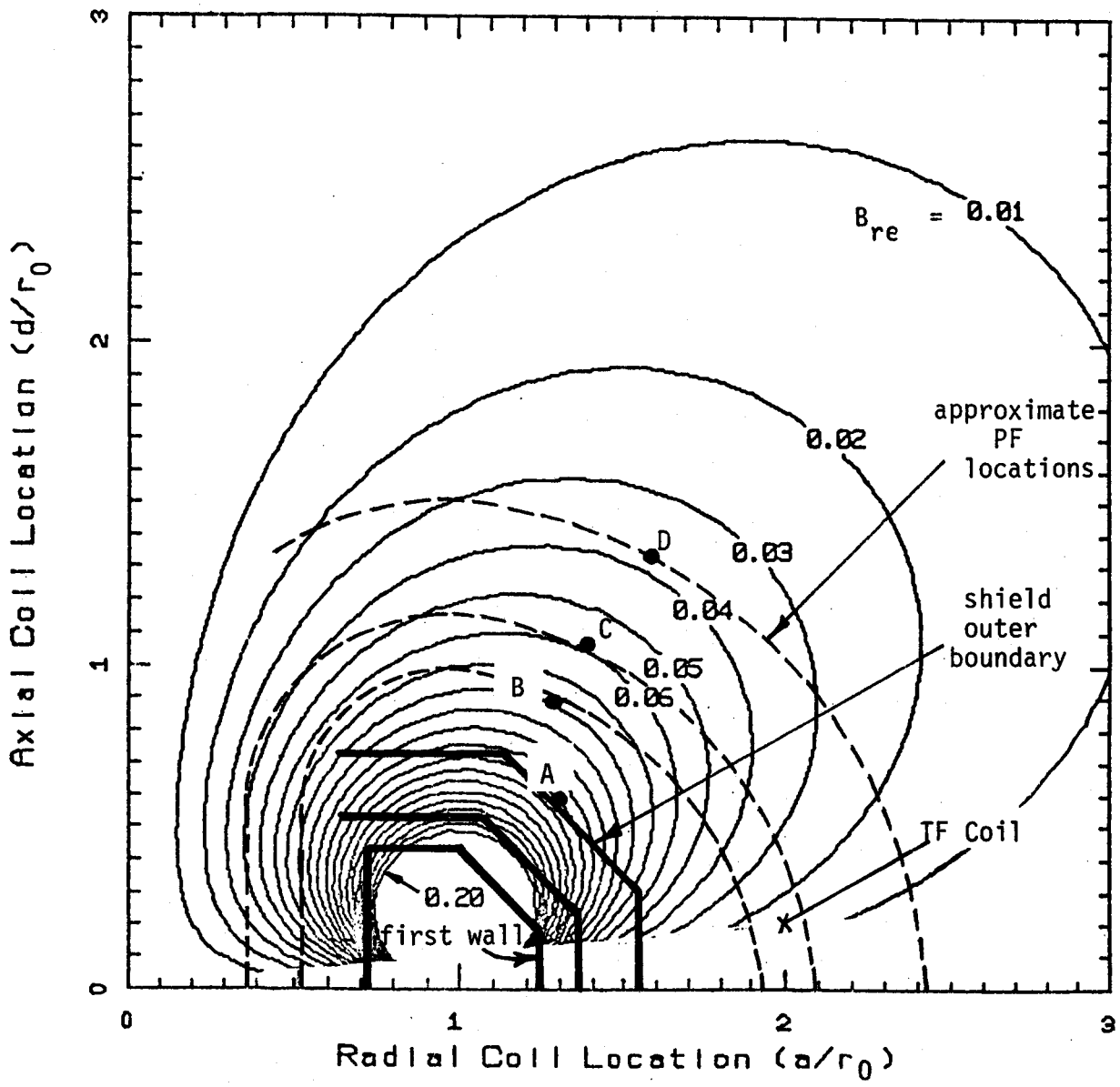

Figure 4.1 - INTOR boundaries superimposed on Contours of Constant B_{re} (Figure 2.2). Points show most effective locations along each boundary.

TABLE 4.1

ENERGY AND POWER FOR VERTICAL STABILIZATION
(FIGURES 2.2 AND 4.1)

1. Points	A	B	C	D
2. Locations	Shield Outer Boundary	TF Coil Plasma Side	TF Coil Outside	PF Coil Boundary
3. Coil Radius, a[m] (1)	6.89	6.94	7.42	8.48
4. Coil z-Location, d[m] (1)	3.18	4.77	5.78	7.16
5. B_{re} (2)	.12	.079	.058	.037
6. Stored Energy, E_o[MJ] (3),(8)	.41	.95	1.76	4.33
7. B_{rp} (4)	.09	.06	.041	.028
8. Time Constant, τ_o[s]	1.0	1.27	1.46	1.91
9. Average Power, P[MW] (6),(8)	0.86	1.91	3.58	5.87
10. Maximum Power, P_p [MW] (7),(8)				
t_w = .01	82.8	191	354	871
= .05	17.2	39.5	72.8	178
= .10	9.00	20.5	37.6	91.1
= .50	2.46	5.30	9.45	21.9

(1) r_o = 5.3 m

(2) Fig. 4.1

(3) Eq. 1 ; B_r = .01 T

(4) Fig. 4.2

(5) Fig. 2.3

(6) Eq. 3 $\rho_{es} = 1.724 \times 10^{-8}$ Ω-m; $A_c = \pi r_w^2 = \pi(r_w/a)^2 a^2, (r_w/a = .0125)$; B_r = .01 T

(7) Eq. 17; B_r = .01 T

(8) Scales by $(B_r/.01)^2$

found by Equation (1). The energies are given on the sixth line for a radial field of 0.01 T. If a different radial field is required these energies would scale by $(B_r/.01)^2$.

Figure 4.2 shows contours of constant radial field normalized to average power for a cycled system. The four boundaries are also shown, with the four points A, B, C and D from Fig. 4.1. The seventh line of Table 4.1 gives the value of the dimensionless radial field produced by coils at these points.

The time constants associated with charging the coil pairs is given by $\tau_o = \mu_o \sigma a^2 G_6$ where G_6 is given in Fig. 2.3 as a function of d/a, and r_w/a. The four time constants for an $r_w/a = .0125$ are listed in line 8 and are based on copper. Lower values are possible with lower (r_w/a) or higher ρ_{es}. Continuous loops are assumed. If saddle coils are used, the time constants, τ_o, will decrease by a factor of 2 - 3 and the peak power will increase somewhat.

The average power required to produce a specified cyclic radial field can be found from Equation (3) if eddy current losses are neglected. Line nine in Table 4.1 gives this average power estimate for the four sets of loops with a resistivity of copper ($\rho_{es} = 1.724 \times 10^{-8}$ Ω-m), an $(r_w/a) = .0125$ and a required field of .01 T. This power will scale by $(B_r/.01)^2$ for other field values.

Finally, (17) is used for line ten which shows the maximum power to charge the coils to produce a stabilizing field of $B_d = 0.01$ T in a time, t_w. For this to occur, it is necessary for a passive stabilizing system to have a time constant $\tau_2 = t_w$.

The values in line 10 also assume that the active coils are complete, toroidally continuous, loops. If saddle coils are formed for the point A,

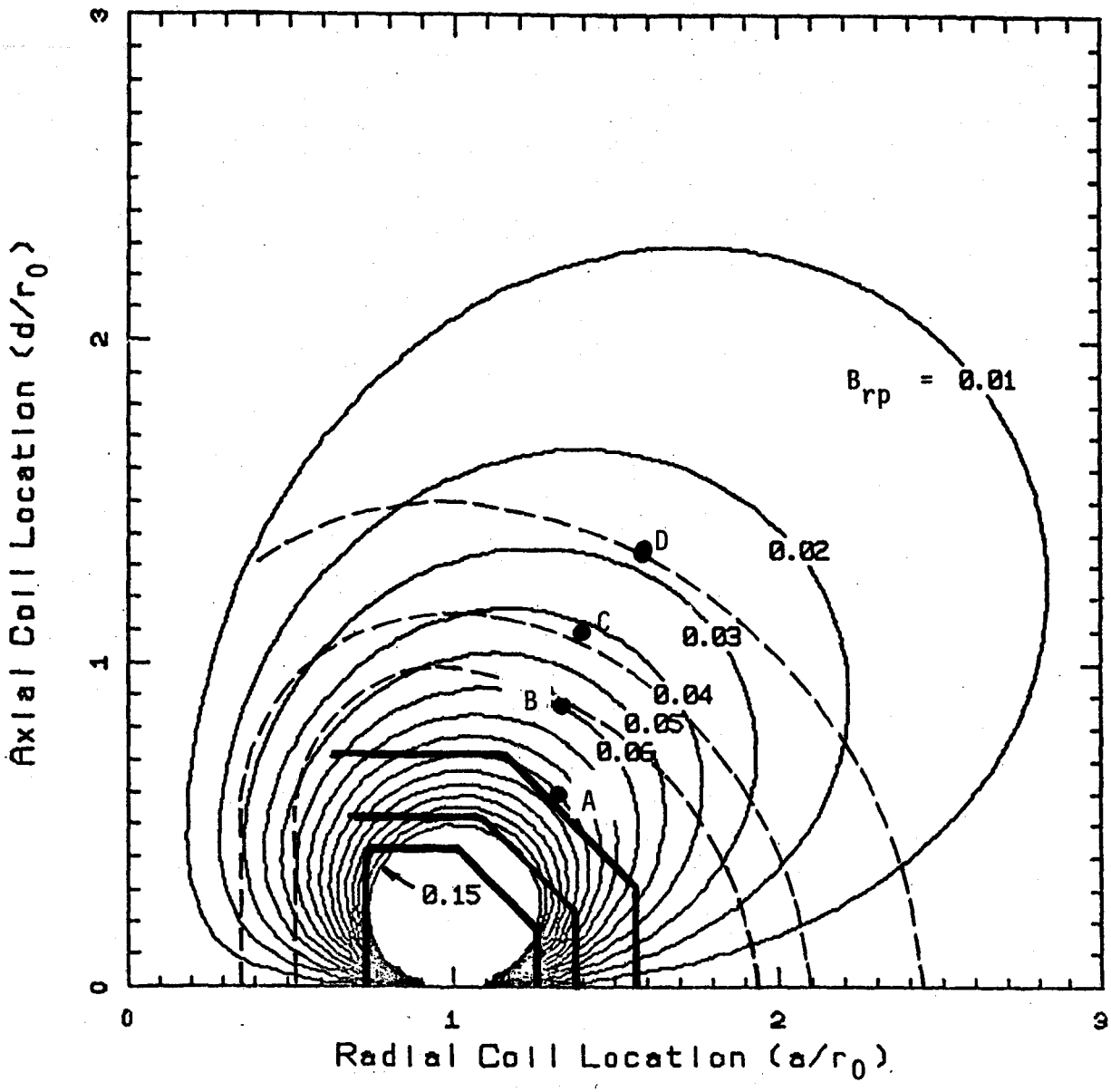

Figure 4.2 - Location of Points from Figure 4.1 on Contours of Constant radial field normalized to average power; (eddy current losses neglected).

the time constant τ_o becomes 0.38 sec and the maximum power for t_w = 0.01, 0.05, 0.10 and 0.50 sec in line 10 becomes 84.1, 18.5, 10.3, and 3.80 MW, respectively.

The table shows that the required energy and maximum power increase by an order of magnitude for an external coil located on the locus of the PF coils relative to an internal coil located at the most effective point on the shield outer boundary. The maximum power for any of the points decreases sharply as t_w increases thus implying the desirability of using a passive stabilizing system with a long time constant. However, the latter will increase the energy requirements for providing the start-up voltage, hence a trade-off is necessary. This will be considered in a later section.

4.2 Radial Stabilization

Figure 4.3 shows contours of constant dimensionless axial field produced by a pair of coils with the four boundaries of interest superimposed on them. The points denoted by A′,B′, C′, and D′ are those locations on the boundaries where a coil should be placed in order to produce the maximum z-directed field at the plasma center for a given stored energy in the coil pair. Although, more effective locations exist below the line $\eta = d/r_o = .44$, this region was excluded in order to allow radial access for other systems.

Table 4.2 identifies the four points and their axial and radial coordinates for an assumed plasma major radius of 5.3 m. The value of the normalized axial field component from Fig. 4.3 is listed in line five.

The energy stored in the coil pairs for a desired axial field at the plasma of .01 T is given in line six. As can be seen in Eq. (4), if other field levels are required, the energies scale by the ratio $(B_z/.01)^2$.

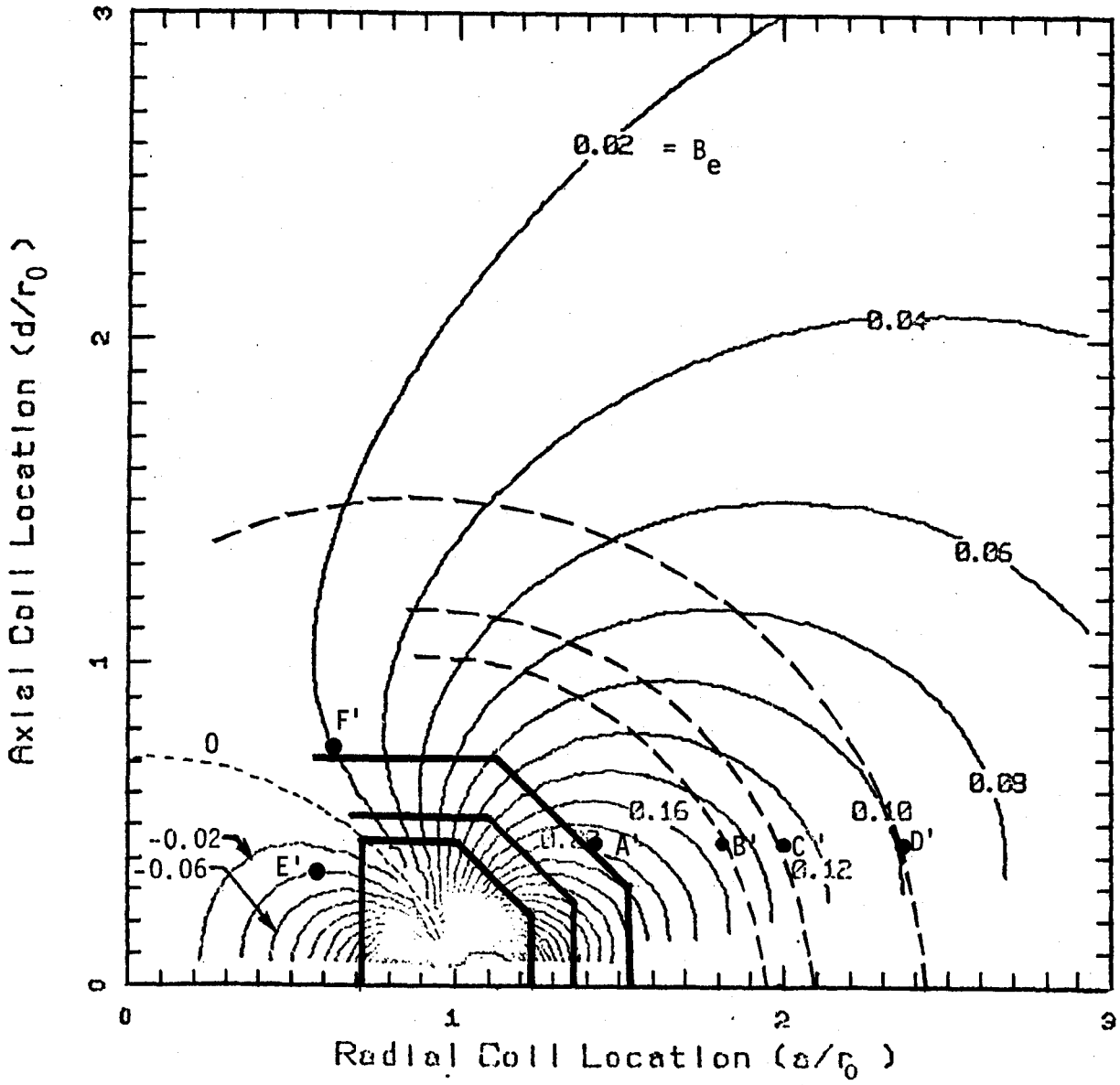

Figure 4.3 - INTOR boundaries superimposed on Contours of Constant B_e (Figure 2.5). Points show most effective radial stabilization locations along each boundary.

TABLE 4.2

ENERGY AND POWER FOR RADIAL STABILIZATION
(FIGURES 2.5 and 4.3)

1. Points	A'	B'	C'	D'
2. Locations	Shield Outer Boundary	TF Coil Plasma Side	TF Coil Outside	PF Coil Boundary
3. Coil Radius, a [m](1)	7.53	9.59	10.49	12.51
4. Coil z-Location, d [m](1)	2.33	2.33	2.33	2.33
5. B_e(2)	.20	.15	.13	.099
6. Stored Energy, E_o [MJ](3),(8)	1.48	2.63	3.51	6.04
7. B_p(4)	.155	.121	.109	.081
8. Time Constant, τ_o' [s](5)	1.92	3.17	3.94	6.02
9. Average Power, P [MW](6),(8)	0.24	0.39	0.49	0.88
10. Maximum Power, P_p [MW](7,8)				
t_w = .01	298	528	704	1210
= .05	60.7	107	142	244
= .10	31.1	54.3	72.0	123
= .50	7.46	12.2	15.8	26.2

(1) r_o = 5.3 m

(2) Fig. 4.3

(3) Eq. (4); B_z = .01 T

(4) Fig. 4.4

(5) Fig. 2.3

(6) Eq. 6; $\rho_{es} = 1.724 \times 10^{-8}$ Ω-m; $r_w/a = 0.125$; B_z = .01 T

(7) Eq. 17; $\tau_1 \rightarrow \tau_o'$; B_z = .01T

(8) Scales as $(B_z/.01)^2$

Figure 4.4 shows contours of constant axial field component normalized to the average power for a cycled system. The four points A′, B′, C′ and D′ are located as Fig. 4.3 - i.e., to produce the maximum axial field component for a given stored energy. The values of the dimensionless radial field normalized to average power are given in line seven in Table 4.2.

Line eight gives the time constants associated with the charging of the coil pairs assuming toroidally continuous loops. These constants are given by $\tau_o' = \mu_o \sigma a^2 G_6'$ where G_6' is given in Fig. 2.3. These time constants are for copper coils with an assumed $r_w/a = .0125$. Lower values are possible with lower (r_w/a) or higher ρ_{es}.

If segmented coils are used for internal coils, for example, they must be formed from 4 loops as illustrated schematically in Fig. 4.5. The most desirable location for the small radius loop to return the current from A′, would be on a negative contour such as point E′ since the return current would then provide an additive field to that produced by A′. Negative contours are, however, in regions where coils may be difficult to locate because of interface constraints. In that case, the return leg should be positioned on the smallest possible contour value since return currents for A′ on positive contours will subtract from the field produced by A′. A return loop at F′, for example, would have a relatively small effect on the field produced by A′, since the contour at F′ has a value of 0.02 whereas the contour at A′ has a value of 0.20. The segmented coils would have a time constant which would be about 0.45 sec rather than the 1.92 sec given in Table 4.2 for complete loops at A′. These represent upper limits based on copper coils and could be reduced by using higher resistance materials or smaller current carrying cross-sections.

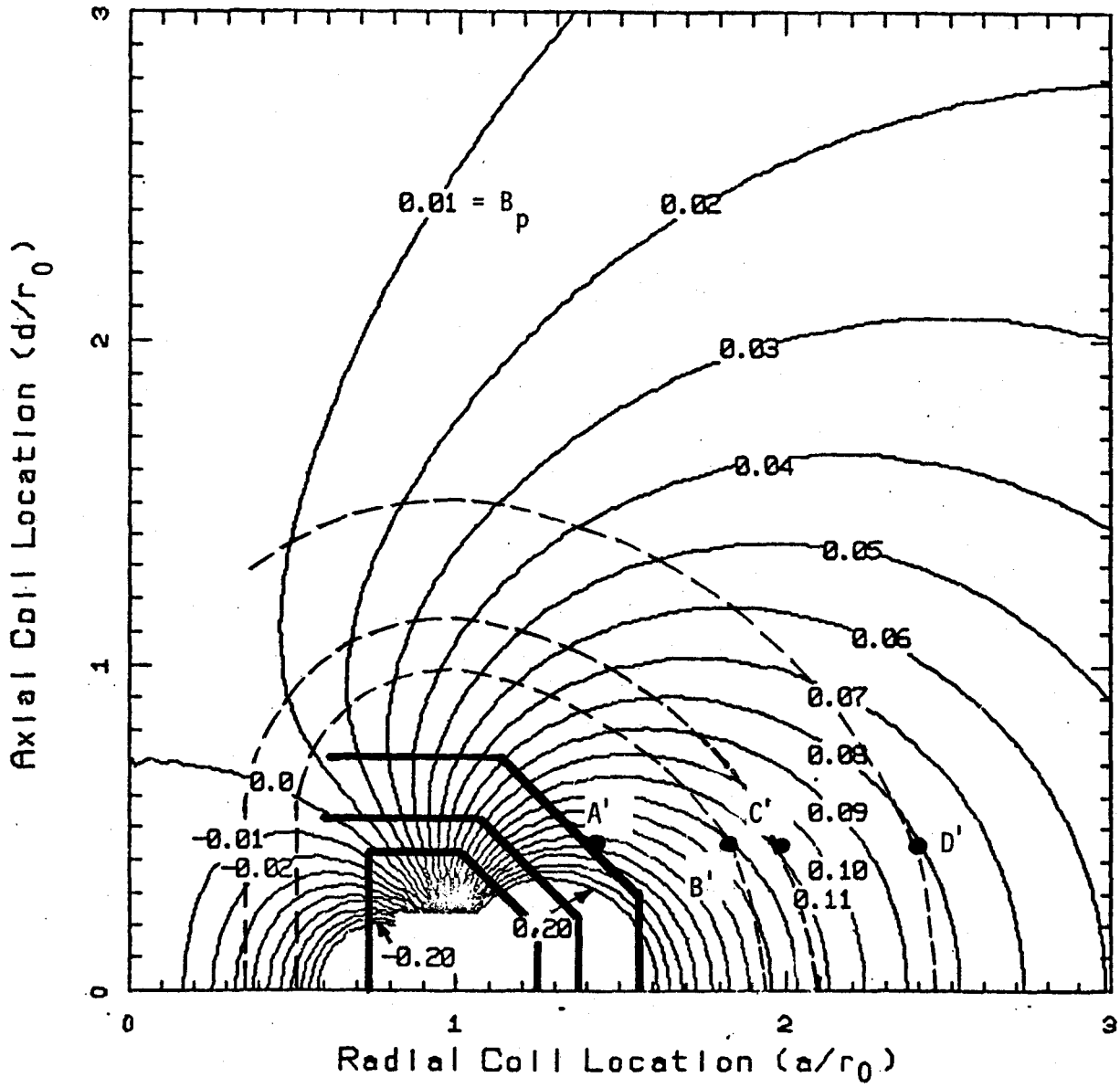

Figure 4.4 - Location of Points from Figure 4.3 on Contours of Constant Axial Magnetic Field normalized to average power.

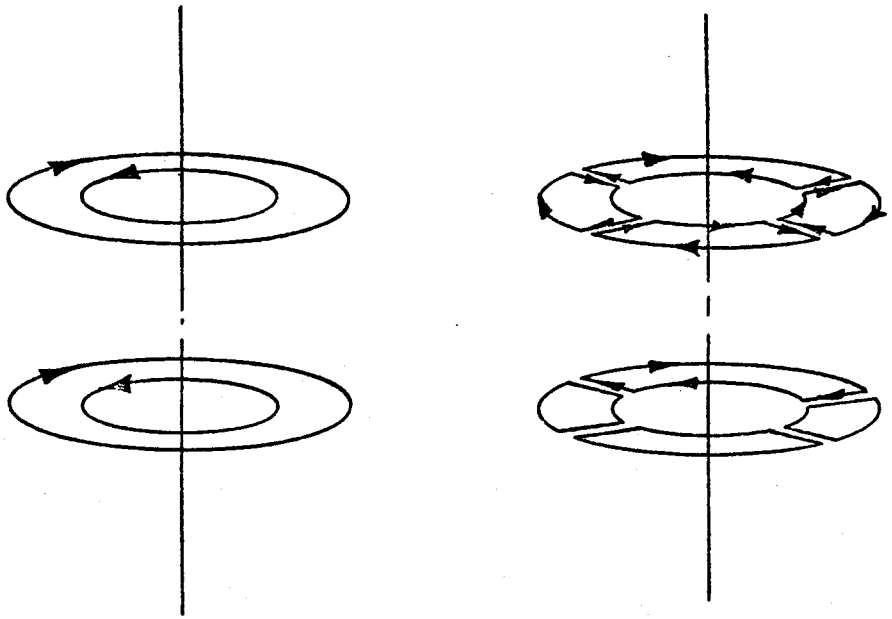

4 Loops with Toroidal Continuity

4 Loops from Coil Segments

Figure 4.5 Active Radial Stabilizing Coils may have toroidal continuity (i.e. - complete loops) or may be formed from coil segments.

In Table 4.2, the average power required to produce a specified cyclic axial field for two loops can be found using Eq. (6) and Fig. 4.5. Line nine gives the average power for the four sets of loops assuming copper ($\rho_{es} = 1.724 \times 10^{-8}$ Ω-m), an $(r_w/a) = .0125$ and a required field of .01 T at the plasma. This power will scale by the ratio $(B_z/.01)^2$ for other field levels.

Finally, Eq. (17) can be used to estimate the maximum power (line 10, Table 4.2) required at time t_w while charging at a constant $\dot{I}$ to produce the required axial field of .01 T. If saddle coils are used for coils at A′, then the change in time constant leads to an increase in maximum power to 303, 65.7, 36.1, and 12.5 MW for $t_w = 0.01$, 0.05, 0.10, and 0.50 sec, respectively.

The values given in line 10 assume that a passive stabilizing system is present with $\tau_2 = t_w$ as described in Section 3.1.2. The energy input is approximately the same as E_o in line 6 since $t_w << \tau_1 = \tau_o'$. The energy input and maximum power required vary by a factor of four between coils A′ and D′ and the maximum power decreases dramatically as t_w increases as in the previous section. Note that coils A' to D' in this section were located at the best possible position in the allowed region and are not at the same points as A to D in the previous section. The decrease in power for this case as t_w increases must be weighed against the increase in energy which occurs with t_w for start-up voltage assist. The latter is shown in the next section and a trade-off is performed.

4.3 Start-up Voltage

Figure 4.6 shows the contours of constant dimensionless flux produced in the plasma loop by a pair of coils. Also shown are four boundaries of

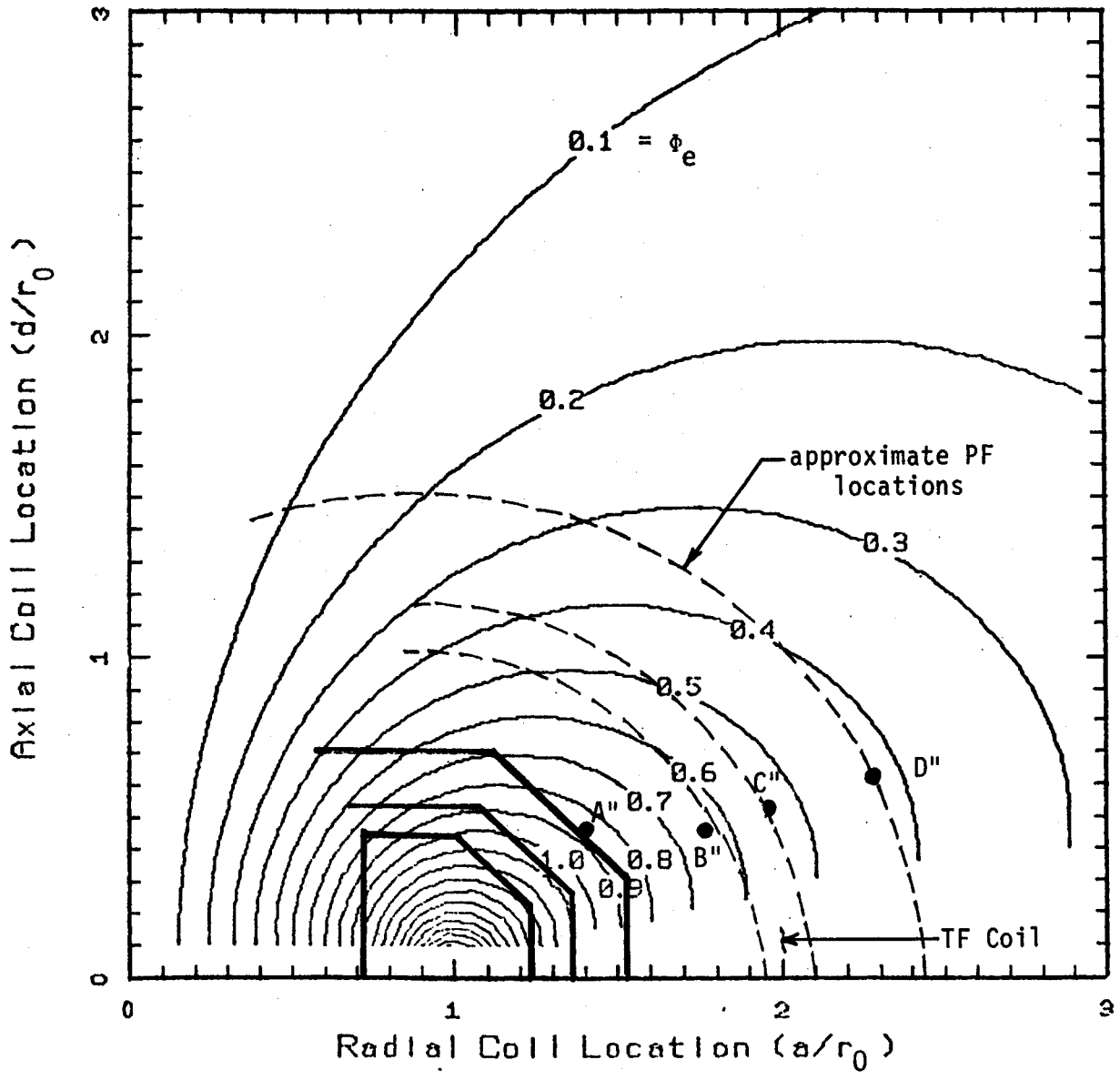

Figure 4.6 - INTOR Boundaries superimposed on Contours of Constant Φ_e (Figure 2.7). Points show most effective locations for producing voltage at the plasma along each boundary.

interest. The point A', B', C', and D' correspond to the locations along the boundaries where a pair of coils should be placed to produce the maximum flux at the plasma for a given stored energy in the coils. Locations below $\eta = d/a = .44$ are ruled out in order to allow radial access for other subsystems.

Table 4.3 gives the locations and coordinates of the four points shown in Fig. 4.6. The fifth line gives the normalized flux produced by coil pairs at the four points.

The time constants associated with charging the coil pairs is given by $\tau_o' = \mu_o \sigma a^2 G_6'$ where G_6' is found from Fig. 2.3. It is assumed that the coils are copper ($\rho_{es} = 1.724 \times 10^{-8}$ Ω-m), with $(r_w/a) = .0125$. The four constants are given in line six. Lower values are possible with lower (r_w/a) or higher ρ_{es}.

Equation (8) relates the voltage $\dot{\phi}$, at the plasma to the dimensionless contours of constant flux, Φ_e, the stored energy and the time, t_o, over which the coils are ramped at a constant $\dot{I}$. For a given $\dot{\phi}$ and t_o, the stored energy in each case can be found from (8). Entry 7 in Table 4.3 lists the energies stored in the loops charged in times of $t_o = .1$, .5 and 1.0 seconds to achieve 25 V (FED) and 100 V (INTOR) at the plasma centers. Other times and/or voltages may be obtained by scaling the entries for $\dot{\phi} = 25$ V, $t_o = .1$ sec by the ratio $(\dot{\phi}\, t_o/2.5)^2$. The total energy input is dependent on $t_o = t_v$; the interval for which the voltage is desired, and on $\Delta t_{\phi s}$, the time lag for flux penetration. The energy input may be estimated using (18), which is plotted in Fig. 4.7. Fig. 4.7 gives the ratio E_{in}/E_o as a function of $(\Delta t_{\phi s}/t_v)$ for selected values of (t_v/τ_1). The graph clearly shows the increase in energy input as the time lag for flux

TABLE 4.3

STORED ENERGY FOR START-UP VOLTAGE

1. Points	A"	B"	C"	D"
2. Locations	Shield Outer Boundary	TF Coil Plasma Side	TF Coil Outside	PF Coil Boundary
3. Coil Radius, a [m](1)	7.42	9.43	10.23	11.93
4. Coil z-Location, d [m](1)	2.33	2.33	2.65	3.18
5. Φ_e(2)	.86	.64	.55	.42
6. Time Constant, τ_o"[s](3)	1.28	2.23	2.63	3.38
7. Stored Energy, E_o [MJ](4)				
$\dot{\phi}$ = 25 V				
t_v = 0.1 sec	.63	1.15	1.55	2.66
= 0.5 sec	16.2	28.9	39.1	66.9
= 1.0 sec	65.5	117	157	269
$\dot{\phi}$ = 100 V				
t_v = 0.1 sec	10.2	18.3	24.8	42.6
= 0.5 sec	258	462	626	1070
= 1.0 sec	1050	1870	2520	4310

(1) r_o = 5.3 m

(2) Fig. 4.5

(3) Fig. 2.3

(4) Eq. 8

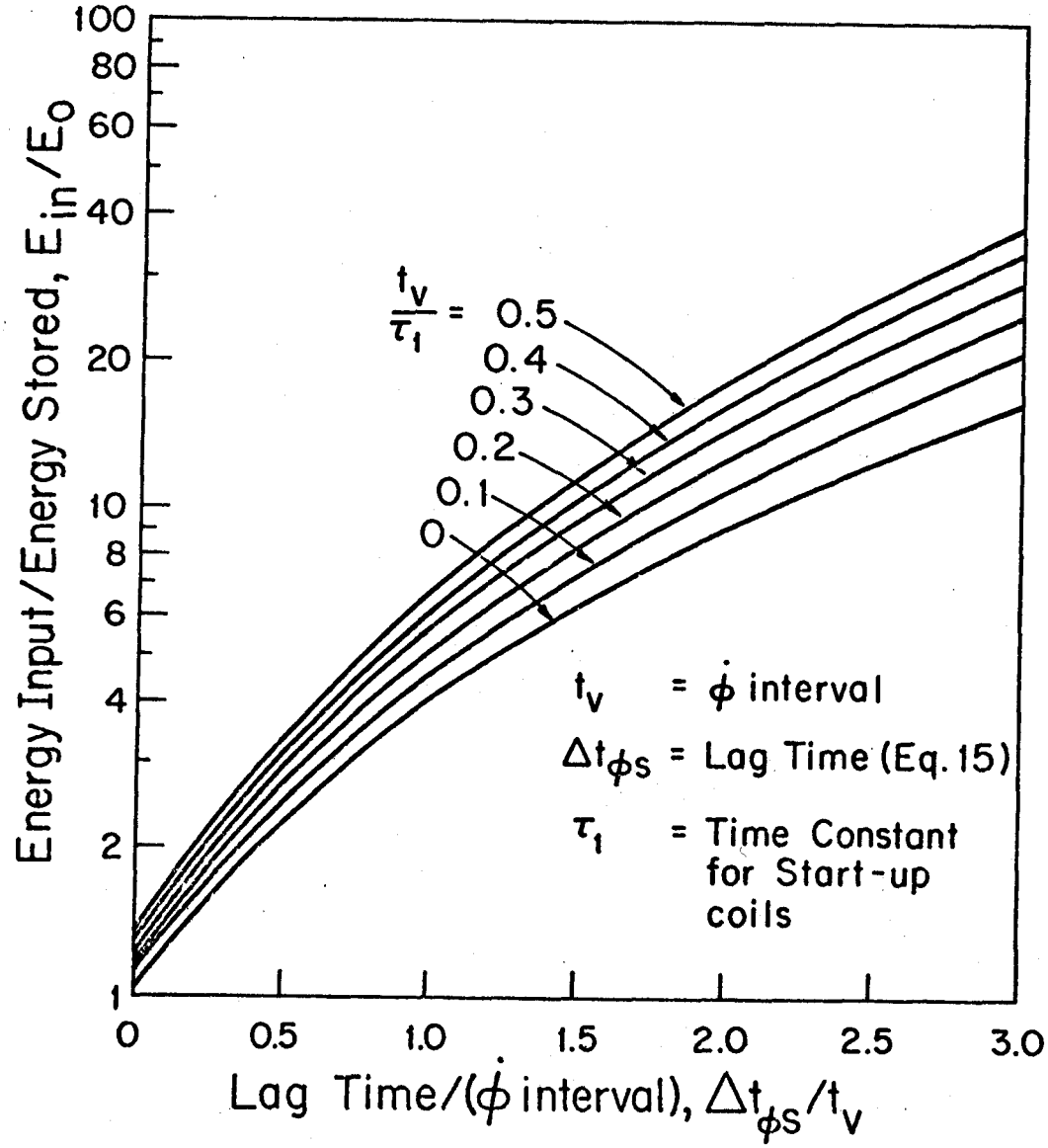

Figure 4.7 Ratio of energy input to stored energy as a function of $\Delta t_{\phi s}/t_v$ for selected values of t_v/τ_1 assuming a constant charge rate for the start-up coils.

penetration increases and may be used to estimate E_{in} for specific cases.

As an example, assume that a start-up voltage of ϕ = 35 V is desired for an interval of t_v = 0.5 sec after the initial transient lag in flux penetration. Results in Table 3.2 showed typically that the lag time $\Delta t_{\phi s}$ was in the range of 0.075 to 0.300 sec. This determines $\Delta t_{\phi s}/t_v$ to use for location along the horizontal axis in Fig. 4.7. Now consider coils A" and D" in Fig. 4.6. The coil location determines its time constant τ_1 (= τ_o'' in Table 4.3). The ratio t_v/τ_1 can now be found and E_o can be determined from (8). The energy input can then be found from (18) or from the ratio E_{in}/E_o from Fig. 4.7. Results for this case are plotted in Fig. 4.8 as a function of the time constant, τ_2, for passive stabilization where it has been assumed that $\Delta t_{\phi s} = 3\ \tau_2$. The curves indicate that the external coils at D" require ~ 3 - 3.5 times the energy input to provide the 35 volts for start-up regardless of the time constant for passive stabilization. The energy input required in either case, however, increases substantially as the time constant for the passive stabilization system increases.

The increase in cost of the energy source for start-up as τ_2 increases must be traded off against the decrease in cost of the power supply for active stabilization as τ_2 increases. The peak power required for vertical stabilization is shown in Fig. 4.9 for coils at A or at D (Table 4.1) in Fig. 4.1. The coils at D are external and assumed to be toroidally continuous loops. The coils at A are internal and are, therefore, shown for two cases: continuous loops or segmented into 12 saddle coils. Saddle coils at A require somewhat more power than continuous loops at A, but are advantageous from the maintenance and assembly standpoint. The external coils at D require about an order of magnitude more power than the continuous

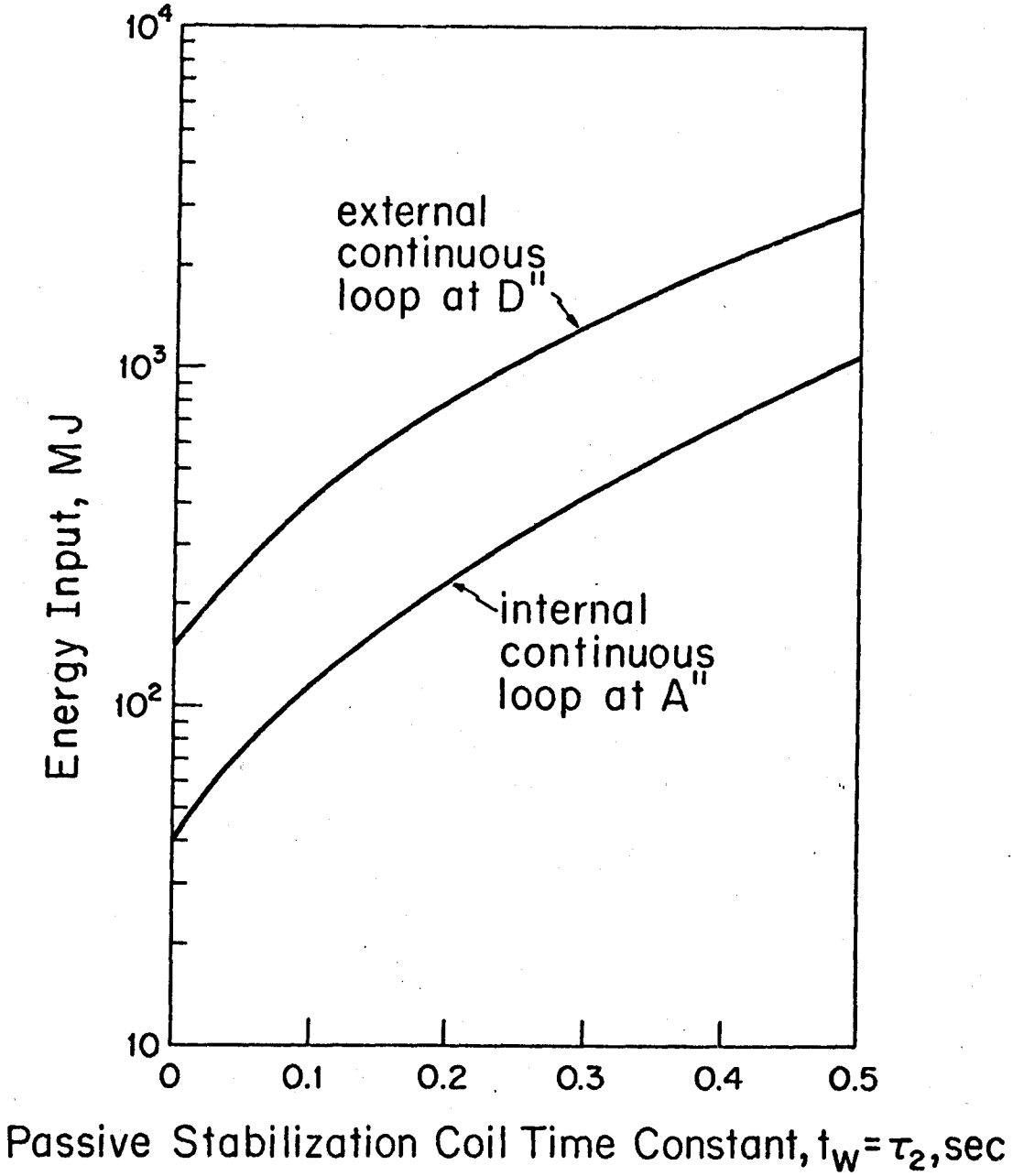

Figure 4.8 Energy Input to Start-up Coils Located in Figure 4.6 to provide a plasma $\dot{\phi}$ = 35 V for 0.5 sec after a lag time $\Delta t_{\phi s} = 3\ \tau_2$.

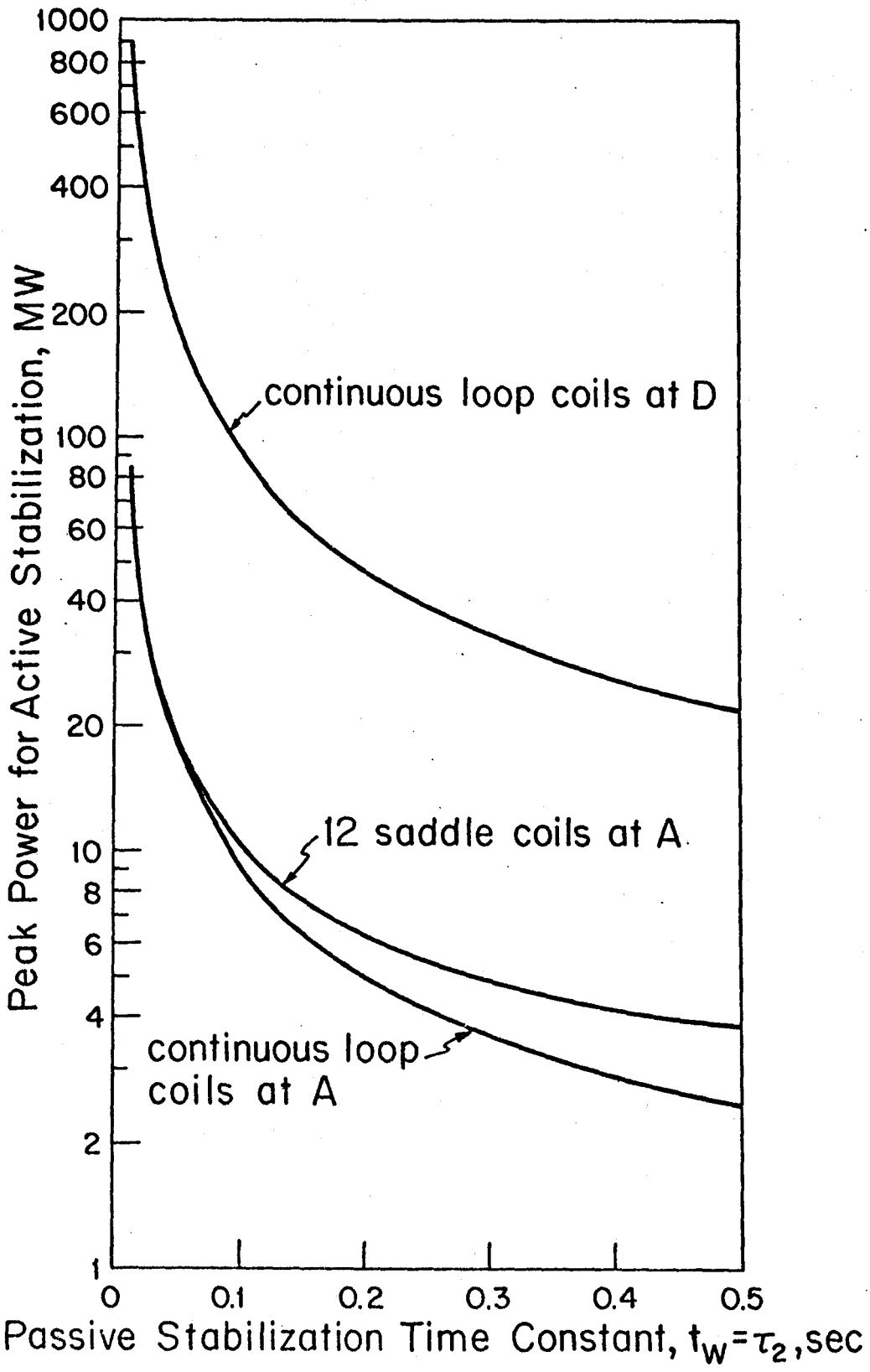

Figure 4.9 Estimated Peak Power Required for Active Vertical Stabilization as a Function of the Time Constant for the Passive Stabilization System (assumes B_r = 0.01 T and coil locations as in Figure 4.1).

loops at A regardless of the passive stabilization time constant. Power requirements decrease substantially over the lower range of τ_2.

A similar plot is given in Figure 4.10 for active radial stabilization coils based on A' and D' in Figure 4.3 and Table 4.2. In this case the continuous external coils at D' require ~3.5 - 4 times the power required for continuous internal coils at A'. The segmented configuration for internal coils is based on coil sections through points A' and F' in Figure 4.3. For all cases, power decreases substantially over the lower range of passive stabilization system time constant.

Figures 4.8 through 4.10 illustrate the strong dependence of the energy input for start-up and the peak power required for active stabilization on the time constant, τ_2, for the passive stabilization system and on whether coils are internal or external. The selection of τ_2 depends on the relative cost of the two sources, but the results in Figures 4.8 - 4.10 imply that a value of τ_2 = 0.200 sec would be consistent with saving energy and peak power.

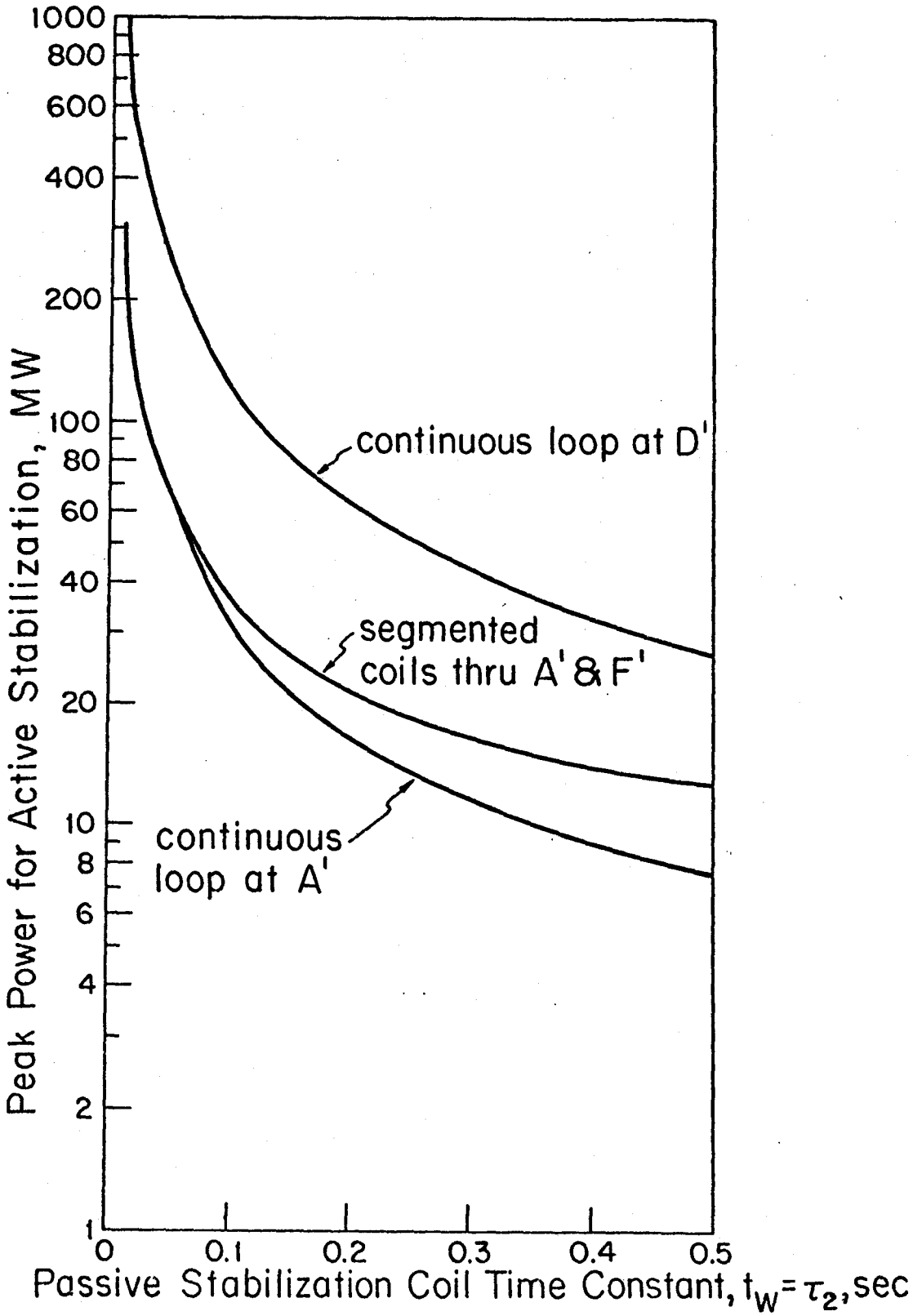

Figure 4.10 Estimated Peak Power Required for Active Radial Stabilization as a Function of the Time Constant for the Passive Stabilization System (assumes B_z = 0.01T and coil locations as in Figure 4.3).

PFC BASE MAILING LIST

Argonne National Laboratory, TIS, Reports Section
Associazione EURATOM - CNEN Fusione, Italy, The Librarian
CRPP, Switzerland, Troyon, Prof. F.
Central Research Institute for Physics, Hungary, Preprint Library
Chinese Academy of Sciences, China, The Library
Eindhoven University of Technology, Netherlands, Schram, Prof. D. C.
The Flinders University of S.A., Australia, Jones, Prof. I.R.
General Atomic Co., Overskei, Dr. D.
International Atomic Energy Agency, Austria,
Israel Atomic Energy Commission, Soreq Nucl. Res. Ctr., Israel
JET, England, Gondhalekar, Dr. A.
Kernforschungsanlage Julich, FRG, Zentralbibliothek
Kyushu University, Japan, Library
Max-Planck-Institut fur Plasma Physik, FRG, Main Library
Nagoya University, Institute of Plasma Physics, Japan
Physical Research Laboratory, India, Sen, Dr. Abhijit
Rensselaer Polytechnic Institute, Plasma Dynamics Lab.
South African Atomic Energy Board, S. Africa, Hayzen, Dr. A.
UKAEA, Culham Laboratory, United Kingdom, Librarian
Universite de Montreal, Lab. de Physique des Plasmas, Canada
University of Innsbruck, Inst. of Theoretical Physics, Austria
University of Saskatchewan, Plasma Physics Lab., Canada
University of Sydney, Wills Plasma Physics Dept., Australia

INTERNAL MAILINGS

MIT Libraries
Industrial Liaison Office
G. Bekefi, A. Bers, D. Cohn, B. Coppi, R.C. Davidson,
T. Dupree, S. Foner, J. Freidberg, M.O. Hoenig, M. Kazimi,
L. Lidsky, E. Marmar, J. McCune, J. Meyer, D.B. Montgomery,
J. Moses, D. Pappas, R.R. Parker, N.T. Pierce, P. Politzer,
M. Porkolab, R. Post, H. Praddaude, D. Rose, J.C. Rose,
R.M. Rose, B.B. Schwartz, R. Temkin, P. Wolff,
T-F. Yang